Atmospheric
Chemistry
and Physics

How can mountaintop CO_2 observations be used to constrain regional carbon fluxes?

John C. Lin[1], **Derek V. Mallia**[1], **Dien Wu**[1], **and Britton B. Stephens**[2]

[1]Department of Atmospheric Sciences, University of Utah, Salt Lake City, Utah 84112, USA
[2]Earth Observing Laboratory, National Center for Atmospheric Research, Boulder, Colorado 80301, USA

Correspondence to: John C. Lin (john.lin@utah.edu)

Abstract. Despite the need for researchers to understand terrestrial biospheric carbon fluxes to account for carbon cycle feedbacks and predict future CO_2 concentrations, knowledge of these fluxes at the regional scale remains poor. This is particularly true in mountainous areas, where complex meteorology and lack of observations lead to large uncertainties in carbon fluxes. Yet mountainous regions are often where significant forest cover and biomass are found – i.e., areas that have the potential to serve as carbon sinks. As CO_2 observations are carried out in mountainous areas, it is imperative that they are properly interpreted to yield information about carbon fluxes. In this paper, we present CO_2 observations at three sites in the mountains of the western US, along with atmospheric simulations that attempt to extract information about biospheric carbon fluxes from the CO_2 observations, with emphasis on the observed and simulated diurnal cycles of CO_2. We show that atmospheric models can systematically simulate the wrong diurnal cycle and significantly misinterpret the CO_2 observations, due to erroneous atmospheric flows as a result of terrain that is misrepresented in the model. This problem depends on the selected vertical level in the model and is exacerbated as the spatial resolution is degraded, and our results indicate that a fine grid spacing of ~ 4 km or less may be needed to simulate a realistic diurnal cycle of CO_2 for sites on top of the steep mountains examined here in the American Rockies. In the absence of higher resolution models, we recommend coarse-scale models to focus on assimilating afternoon CO_2 observations on mountaintop sites over the continent to avoid misrepresentations of nocturnal transport and influence.

1 Introduction

Scientific consensus among climate scientists points to carbon dioxide (CO_2) as the main greenhouse gas leading to climate change (IPCC, 2014). Therefore, a strong need exists to quantify and understand global carbon fluxes, among which the terrestrial biospheric component is the most dynamic, potentially even reversing signs on an annual basis from year to year (Le Quéré et al., 2015; Sarmiento et al., 2010). Yet quantifying and predicting terrestrial biospheric carbon fluxes continue to pose a challenge to researchers, as seen in the large divergence between models in projections of biospheric fluxes into the future (Cox et al., 2000; Friedlingstein et al., 2003; Arora et al., 2013) as well as in hindcast mode, particularly at the regional scale (Sarmiento et al., 2010; Stephens et al., 2007; Fisher et al., 2014).

Because mountains cover approximately a quarter of the Earth's land surface (Blyth et al., 2002), it is imperative to quantify and understand carbon fluxes over "complex terrain". Case in point is the western US, where significant amounts of biomass are found above 1000 m elevation (Fig. 1). Similarly, much of the biomass and potential for terrestrial carbon storage in other parts of the world are found in hills or mountains, partly due to the fact that historical deforestation and biomass removal have been most pronounced in easier-to-access, flat regions (Ramankutty and Foley, 1999).

Despite the importance of regions with complex terrain in regional to global carbon cycling, these areas have hitherto been under-sampled due to logistical difficulties, harsh environmental settings, and violation of flat terrain assumptions in eddy covariance. Recently, Rotach et al. (2014) argued that current difficulties to balance the terrestrial carbon budget are
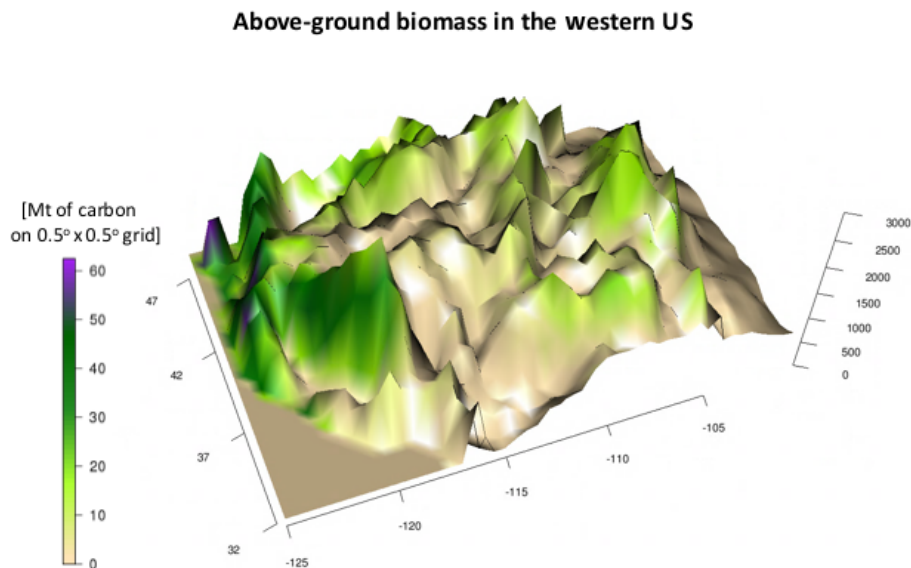
Above-ground biomass in the western US

Figure 1. Above-ground biomass (megatons, Mt, of carbon) from the North American Carbon Program baseline dataset for year 2000 (Kellndorfer et al., 2013) overlaid on topographic surface in the western US, resolved at $0.5° \times 0.5°$ grid spacing.

due to inabilities to handle atmospheric circulations in complex terrain. While these authors presented a strong case for the consideration of flows over complex terrain, they did not quantify the implications of neglecting such flows for interpreting CO_2 observations. However, the significance of complex terrain has led to efforts to start closing this gap, in regions such as Europe (Pillai et al., 2011) and the American Rockies (Schimel et al., 2002); see below.

The American Rockies will be the focus region of this study, which attempts to show how CO_2 concentrations in mountain regions can be properly linked, through atmospheric transport, to biospheric fluxes. While the objective of this paper is to use the American Rockies as a case study to illustrate general aspects of interpreting CO_2 observations in mountainous regions, several other compelling reasons exist for studying this region. Both models and observations have suggested that significant carbon storage can occur in the American Rockies (Fig. 1; Schimel et al., 2002; Monson et al., 2002; Wharton et al., 2012), albeit this storage is highly sensitive to environmental drivers such as temperature and water availability (Monson et al., 2006; Schwalm et al., 2012; Wharton et al., 2012; Potter et al., 2013) as well as disturbances such as insect infestation (Negron and Popp, 2004) and wildfires (Wiedinmyer and Neff, 2007). These disturbances are also coinciding with rapid population increases in this region (Lang et al., 2008), with concomitant rise in urban CO_2 emissions (Mitchell et al., 2017), urban–wildland interfaces (Mell et al., 2010), and demands for water resources (Reisner, 1993; Gollehon and Quinby, 2000).

Recently, several research efforts have attempted to improve the understanding of carbon fluxes in the American Rockies. Direct eddy covariance-based measurements of car-

bon fluxes have been carried out in the mountains (Blanken et al., 2009; Yi et al., 2008); however, the eddy covariance technique characterizes fluxes only over a small area of $\sim 1\,km^2$ (Baldocchi et al., 2001) and requires careful attention to potential biases from local advection. Ground-based ecological measurements (Anderegg et al., 2012; Tkacz et al., 2008) yield detailed information regarding the ecosystem, but such observations are also limited in spatial coverage and temporal resolution. Atmospheric CO_2 observations can characterize fluxes over hundreds of km (Gerbig et al., 2009), providing important regional-scale constraints. Aircraft-based CO_2 measurements in this region have had some success in characterizing regional-scale fluxes (Desai et al., 2011), albeit on a sporadic, campaign-based setting. More significantly, a network of accurate CO_2 observations has been maintained on mountaintops in the Rockies for the past decade (Stephens et al., 2011). These observations have been assimilated by sophisticated global carbon data assimilation systems such as "CarbonTracker" (Peters et al., 2007) to retrieve biospheric carbon fluxes over the mountainous regions and the rest of the globe.

Due to the expanding number of CO_2 observations in mountainous areas and the need to understand carbon fluxes in such regions, a strong motivation exists to evaluate existing methods in which CO_2 observations are used in atmospheric models to retrieve carbon fluxes. Van der Molen et al. (2007) simulated CO_2 variability near a Siberian observational site and showed that even modest terrain variations of $\sim 500\,m$ over 200 km could lead to considerable CO_2 gradients. Due to the dangers of misrepresenting terrain/flows and introducing biases into the carbon inversion system, mountaintop CO_2 observations have often been omitted from car-

bon inversion systems (Rodenbeck, 2005; Geels et al., 2007; Peters et al., 2010). In fact, the most recent release of Carbon-Tracker ("CT-2015") stopped assimilating the three mountaintop sites in the American Rockies (http://www.esrl.noaa.gov/gmd/ccgg/carbontracker/).

However, the absence of mountaintop CO_2 observations to constrain carbon inversion systems is, in effect, throwing away valuable information that could inform carbon exchange in potentially important areas of the world (Fig. 1). Case in point is the Schauinsland CO_2 time series on a mountain in the middle of Western Europe, which as of this writing has collected over 40 years of continuous CO_2 data (Schmidt et al., 2003) but remains excluded from numerous carbon inversion systems (Rodenbeck, 2005; Geels et al., 2007; Peters et al., 2010).

As a means to evaluate models' ability to interpret mountaintop CO_2 observations, we specifically adopt the observed diurnal cycle during the summer growing season as a key diagnostic. This is because the diurnal cycle during the growing season, with nighttime respiratory release and daytime photosynthetic drawdown of CO_2, is a prominent feature in the coupling between biospheric fluxes and the atmosphere and one of the dominant modes in the CO_2 time series (Bakwin et al., 1998; Denning et al., 1996). Furthermore, models tend to either use CO_2 data from the nighttime (to sample subsiding air in the mid-troposphere; Keeling et al., 1976) or from the daytime (during well-mixed conditions), and aspects of the diurnal cycle can provide clues as to whether the model is capturing the link between fluxes and concentrations right at either, both, or neither of these times.

The diurnal pattern of CO_2 observed at the Storm Peak Laboratory (SPL), Colorado, was examined by one of the first mesoscale modeling studies that investigated the impact of mountain flows on CO_2 concentrations (De Wekker et al., 2009). Although this study adopted an idealized simulation covering only a single day of observations, it nonetheless underscored the role of daytime upslope winds. A common approach is to assimilate mountain observations at night (Peters et al., 2007), favoring subsidence conditions characterizing free-tropospheric concentrations and avoiding the need to resolve daytime upslope flows (Keeling et al., 1976).

Recently, Brooks et al. (2016) used pseudo-observations to examine the detectability of a regional flux anomaly by three mountaintop CO_2 sites in the American Rockies (including the Storm Peak Laboratory). For the atmospheric model they adopted a time-reversed Lagrangian particle dispersion model (LPDM), which yields the "footprint", or source region, of the observation sites (Lin et al., 2012). Although this study investigated whether the three mountaintop sites could detect signals of ecosystem disturbance, Brooks et al. (2016) did not specifically examine issues related to erroneous atmospheric transport in complex terrain or compare modeled CO_2 against observed values.

In this paper, we will focus on the same three mountaintop CO_2 sites in the American Rockies and specifically examine

the implications of using nocturnal vs. daytime data within models, in light of atmospheric models at various grid spacings – from high resolution regional simulations to coarser global-scale simulations. More specifically, we will drive a time-reversed LPDM with various meteorological fields and receptor heights. We will probe the implications on the footprint, transport, and the resulting CO_2 concentrations as the driving meteorological fields are degraded with coarser grid spacing and also as different vertical levels within the model are used.

The guiding questions of this paper are as follows:

1. How do atmospheric flows in mountainous areas affect CO_2 concentrations and their representation in models?

2. What are the errors incurred due to the use of coarse-scale atmospheric simulations?

3. How can mountaintop CO_2 observations be used in an effective manner to constrain regional carbon fluxes in complex terrain?

2 Methodology

2.1 RACCOON observations

The Regional Atmospheric Continuous CO_2 Network (RAC-COON, http://raccoon.ucar.edu) was established in 2005 and has collected in situ CO_2 measurements at up to six sites over the past decade (Stephens et al., 2011). Here we present and simulate observations from the three longest running high-alpine sites (Fig. 2; Table 1). The easternmost site (NWR) is at 3523 m elevation near the treeline on Niwot Ridge, just west of Ward, CO. Niwot Ridge is an LTER (Long Term Ecological Research network) site and there is an Ameri-Flux tower run by the University of Colorado ~ 5 km east and 500 m lower on the ridge. The instrumentation reside in the "T-Van" where the US National Oceanic and Atmospheric Administration's (NOAA) Global Monitoring Division has collected weekly flask samples for measurement of CO_2, isotopes, and other species for over 40 years, and daily flasks since 2006. The middle site (SPL) is at the Desert Research Institute's Storm Peak Lab (3210 m on Mt. Werner near Steamboat Springs, CO). This mountaintop observatory has a long history of measurements related to cloud physics, cloud–aerosol chemistry, and air quality. The westernmost site (HDP) is on Hidden Peak (3351 m, above the Snowbird ski resort, Utah). This mountaintop site generally experiences regionally well-mixed or free-tropospheric air, but with influences from Salt Lake City during boundary-layer growth and venting periods.

The RACCOON measurements are based on a LiCor LI-820 single-cell IRGA with frequent calibrations. The instruments sample air from one of three inlet lines on a tower (two at HDP) and use a suite of four calibration gases plus
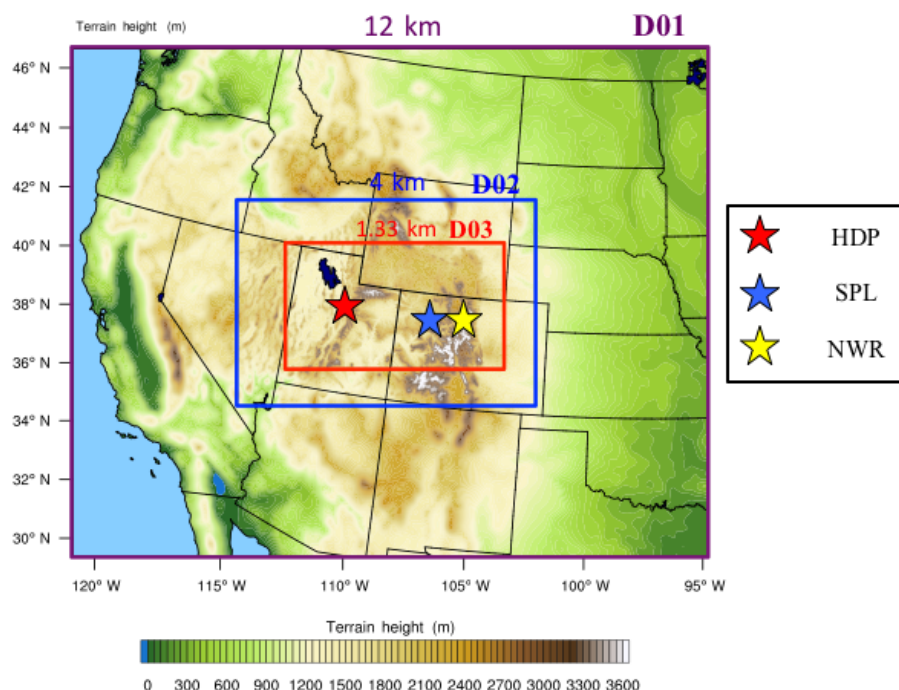
Figure 2. The WRF simulation domain, covering the western US with a series of nests with 12, 4, and 1.3 km grid spacing. These WRF meteorological fields are used to drive air parcel trajectories within the STILT model.

a fifth surveillance gas. All reference gases are rigorously tied to the WMO (World Meteorological Organization) CO_2 calibration scale with use of the NCAR (National Center for Atmospheric Research) CO_2 and O_2 calibration facility. 100-second average measurement precision is ± 0.1 ppm (1 σ), and inter-comparability is estimated from several methods to be 0.2 ppm (Stephens et al., 2011).

We applied filtering to the mountaintop CO_2 observations to remove local influences and to extract values that are more regionally representative (Brooks et al., 2012). Observations were filtered out in which the within-hour standard deviation is greater than 1.0 ppm or when the differences between the top two inlets are greater than 0.5 ppm, which indicate periods when significant influences that are highly localized to the site are affecting the observations. This filtering removed 15, 16, and 27 % of the hourly observations at HDP, SPL, and NWR, respectively. Regardless, filtering made negligible differences in the observed diurnal cycles in CO_2 (see the Supplement). Henceforth, we will refer to the filtered observations when discussing the observed CO_2.

2.2 WRF–STILT atmospheric model

The atmospheric modeling framework adopted in this study is a Lagrangian time-reversed particle dispersion model, the Stochastic Time-Inverted Lagrangian Transport (STILT)

model (Lin et al., 2003), driven by a mesoscale gridded model, the Weather Research and Forecasting (WRF) model (Skamarock and Klemp, 2008). STILT is a Lagrangian model that simulates the effects of turbulent dispersion using the stochastic motions of air parcels. It has been widely applied to the interpretation of CO_2 and trace gases in general (Lin et al., 2004; Hurst et al., 2006; Göckede et al., 2010; Kim et al., 2013; Mallia et al., 2015; Jeong et al., 2012). WRF is a state-of-the-art non-hydrostatic mesoscale atmospheric model that can simulate a variety of meteorological phenomena (Skamarock and Klemp, 2008), gaining widespread acceptance and usage among the atmospheric science community. Careful coupling between WRF and STILT has been carried out, with an emphasis towards physical consistency and mass conservation (Nehrkorn et al., 2010).

For this study, we ran WRF in a two-way nested mode centered between Utah and Colorado where the RACCOON sites are located (Fig. 2). The grid spacing was refined in factors of 3, from 12 km grid spacing covering the entire western US to 4 km and then to 1.3 km in the innermost domain that covers all of the RACCOON sites. A total of 41 vertical levels were adopted, with 10 of these levels within 1 km of the ground surface, following Mallia et al. (2015). Comprehensive testing of different WRF settings has been carried out as part of a previous publication (Mallia et al., 2015) and adopted here: i.e., the MYJ, Grell–Devenyi en-

Table 1. Characteristics of RACCOON mountaintop sites examined in this paper, as well as the representation of terrain in different meteorological files at these sites.

	Hidden Peak (HDP)	Storm Peak Lab (SPL)	Niwot Ridge (NWR)
Latitude/longitude	40°33′38.80″ N	40°27′00″ N	40°03′11″ N
	111°38′43.48″ W	106°43′48″ W	105°35′ 11″ W
Top inlet height	17.7 m	9.1 m	5.1 m
Site altitude [m a.s.l.]	3351 m	3210 m	3523 m
Site altitude as resolved by models [m a.s.l.]:			
WRF–1.3 km	2996 m	3038 m	3411 m
WRF–4 km	2918 m	2818 m	3382 m
WRF–12 km	2357 m	2724 m	3076 m
GDAS	1856 m	2757 m	2333 m
CarbonTracker	2004 m	2582 m	2276 m

semble, and Purdue Lin schemes for parameterizing the planetary boundary layer (PBL), cumulus convection, and microphysics, respectively. In addition to the testing reported in Mallia et al. (2015), we have also carried out evaluations of the WRF fields specifically using meteorological measurements on mountaintops, near the RACCOON sites. These evaluations reveal that errors in the simulated meteorological fields are reasonable when compared against other atmospheric simulations evaluated in less complex terrain (Mallia et al., 2015), and biases are especially small for the WRF–1.3 km fields (Table 2). In this paper, we will examine the resulting differences in meteorological and CO$_2$ simulations when STILT is driven by WRF fields at three different grid spacings.

In addition to the three WRF domains, we drove STILT with a fourth meteorological field, from NCEP's (National Centers for Environmental Prediction) Global Data Assimilation System (GDAS). GDAS is archived at 1° × 1° grid spacing, at 6-hourly intervals and at 23 vertical pressure levels. Driving STILT with GDAS was a means by which we attempted to construct an atmospheric model to resemble the NOAA CarbonTracker product, which was also at 1° × 1° resolution (and 25 vertical levels) over North America. More details about CarbonTracker can be found in the next section.

Driven by the various meteorological fields, STILT released 2000 air parcels every 3 h (00:00, 03:00, 06:00, …, 21:00 UTC) for the months of June, July, and August 2012 from the RACCOON sites and transported for 3 days backward in time. An example of STILT-simulated air parcel trajectories can be found in Fig. S1. The choice of 2000 parcels followed from results from sensitivity tests in a previous study, also over the western US (Mallia et al., 2015). In the case of WRF, STILT has the capability to transport the parcels in a nested fashion. So when we refer to "WRF 1.3 km simulations", it actually means that the atmosphere in the innermost domain (Fig. 2) was simulated at 1.3 km, switching to 4 km grid spacing when the parcel left the 1.3 km domain; likewise, the 12 km winds were used when

the parcel left the 4 km domain. For the "WRF 4 km simulations" we started with the 4 km fields as the innermost domain and then 12 km in the outer domain.

For each site, we released STILT parcels using two different ways to determine starting levels. When we refer to "AGL", we mean that the starting height was set at the level of the inlet above the ground surface (Table 1), following the local terrain as resolved in the meteorological model (whether at 1.3, 4, or 12 km, or 1° grid spacing). The alternative method, referred to as "ASL", means that the starting level was set to the elevation above sea level. For instance, the HDP site is located at 3351 m above sea level. The ground height as resolved by the 12 km WRF model is at 2357 m, so the starting height was placed at 994 m (= 3351 − 2357) above the resolved terrain. CarbonTracker, as well as many other global-scale models (Geels et al., 2007; Peters et al., 2010), places the observation site at an internal model level following the ASL method, so the "GDAS–ASL" runs were a means by which we attempted to mimic the global model configuration and to illuminate potential errors that could result from such a configuration. We also tested the AGL height for GDAS, at HDP only. As shown later, these runs were highly erroneous, so we did not carry them out for the other two sites.

The STILT-simulated air parcels were tracked as they were transported backwards in time from the RACCOON receptors (see example in Fig. S1); when they were in the lower part of the PBL, the locations of the parcels and amount of time the parcels spent in the lower PBL were tallied. This information was used in calculation of the footprint – i.e., the sensitivity of the receptor to upwind source regions (in units of concentration per unit flux). For more details, see Lin et al. (2003). The footprints, encapsulating the atmospheric transport information, were then combined with gridded fluxes from the biosphere and anthropogenic emissions, which are described in the next sections.

Table 2. Comparisons of different meteorological files driving STILT against hourly averaged wind observations at the Storm Peak Laboratory ($-106.74°$ W; $40.45°$ N) and at Niwot Ridge ($-105.586°$ W; $40.053°$ N; 3502 m a.s.l.; Knowles, 2015), near the RACCOON CO_2 site. Meteorological observations were not available at the Hidden Peak site. Error statistics are presented separately for the west-to-east component ("u-wind") and south-to-north component ("v-wind") of the wind velocity vector.

Site	SPL				NWR			
Run type	1.3 km WRF	4 km WRF	12 km WRF	GDAS	1.3 km WRF	4 km WRF	12 km WRF	GDAS
u-wind BIAS [m s^{-1}]	-0.5	-1.5	-0.9	2.3	0.1	-0.3	-1.4	-0.2
v-wind BIAS [m s^{-1}]	-0.6	-0.3	-0.2	1	0.2	0.4	0.9	1.1
u-wind RMSE [m s^{-1}]	3.1	3.8	3.2	3.7	3.5	3.4	3.4	3.2
v-wind RMSE [m s^{-1}]	2.7	2.7	2.3	2.5	2.2	2.1	2.2	3

2.3 CarbonTracker CO_2 concentrations and biospheric fluxes

CarbonTracker is a carbon data assimilation system covering the whole globe that retrieves both oceanic and terrestrial biospheric carbon fluxes (Peters et al., 2007). Observed atmospheric CO_2 concentrations are assimilated by CarbonTracker, which adjusts carbon fluxes to minimize differences with the observed CO_2 using an ensemble Kalman filter methodology.

We took three-dimensional CO_2 fields from CarbonTracker to initialize CO_2 concentrations at the end of the 3-day back trajectories from STILT. CarbonTracker-derived biospheric fluxes, along with anthropogenic and fire emissions (Sect. 2.4), were also multiplied with STILT-derived footprints and combined with the initial CO_2 concentrations to yield simulated CO_2 at the RACCOON receptors.

CarbonTracker is maintained and continues to be developed by the NOAA's Earth System Research Laboratory. For this paper, we adopt the "CT-2013b" version. CT-2013b provides multiple prior estimates of the oceanic, terrestrial, and fossil carbon fluxes, with each combination yielding separate posterior fields of carbon fluxes and CO_2 distributions. CT-2013b results are presented as an average across the suite of prior fluxes and CO_2 fields.

CT-2013b resolves atmospheric transport and fluxes at $1° \times 1°$ over North America and $3°$ long $\times 2°$ lat in the rest of the globe, with 25 vertical levels. The driving meteorological fields come from the European Centre for Medium-Range Weather Forecasts's ERA-Interim reanalysis. The ensemble Kalman filter system within CarbonTracker solves for scaling factors on weekly timescales to adjust upward or downward biospheric carbon fluxes. The adjustments were made over "ecoregions" on land, rather than attempting to adjust fluxes within individual grid cells, as a way to reduce the dimensions of the inversion problem within CarbonTracker. More details regarding the CarbonTracker system can be found in Peters et al. (2007) and online at http://www.esrl.noaa.gov/gmd/ccgg/carbontracker/CT2013B/.

Since CarbonTracker was designed for global carbon cycle analyses to retrieve large-scale fluxes, the adjustment to

biospheric carbon fluxes could result in artifacts at the local to regional scales. More specifically, the attempt to match CO_2 observations with a single scalar can result in flipped diurnal cycles, causing carbon uptake during the night that is partly offset by enhanced respiration in a nearby ecoregion (Fig. S2). For this paper, we implemented a fix that removed this artifact by detecting these reversed diurnal patterns, adjusting them while preserving the 24 h integrated carbon flux. See the Supplement and Fig. S3 for details.

2.4 Anthropogenic and fire emissions

Anthropogenic CO_2 emissions were obtained from the Emission Database for Global Atmospheric Research (EDGAR; European Commission, 2009), which resolves emissions globally at $0.1° \times 0.1°$ annually. In order to temporally downscale the annual emissions, hourly scaling factors were obtained from the Vulcan emission inventory (Gurney et al., 2009) and applied to the EDGAR annual emissions. Lastly, CO_2 emissions from EDGAR for year 2010 were extrapolated to 2012 using population growth rates across the US since 2010, as this was the last year in which EDGAR emissions were available.

Wildfire emissions for CO_2 were obtained from the Wildland Fire Emissions Inventory (WFEI; Urbanski et al., 2011). Since these emissions were only reported daily, 3-hourly diurnal scaling factors were obtained from the Global Fire Emissions Database v3.1 and applied to the daily WFEI emissions to downscale the emissions to sub-daily timescales (Mu et al., 2011; van der Werf et al., 2010).

Contributions from anthropogenic and wildfire emissions, on average, to the mean CO_2 diurnal cycle observed at all the mountain sites were secondary in comparison to the biosphere (Fig. S4). In particular, the wildfire contributions were episodic and averaged out to negligible contributions over June–August 2012 (Fig. S4). Because of this, we will not touch upon wildfires in the remainder of the paper.
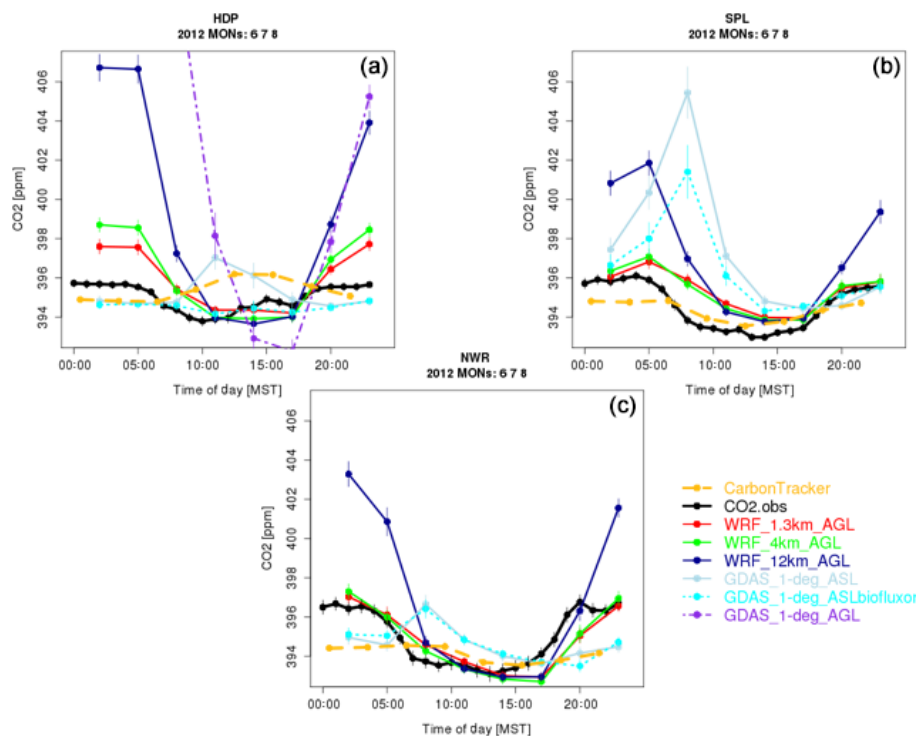
Figure 3. The average diurnal CO_2 pattern during June–August 2012 as observed at the three mountaintop sites in the RACCOON network: Hidden Peak (HDP), Storm Peak Laboratory (SPL), and Niwot Ridge (NWR). Compared against the observations are simulated diurnal CO_2 patterns from different models: CarbonTracker, STILT driven with WRF at different grid spacings, and STILT driven with GDAS. Multiple GDAS-driven STILT model configurations are shown, including runs without fixes to the biospheric fluxes ("biofluxorig"; see the Supplement) as well as releasing air parcels at the elevations of the sites above mean seal level (ASL) or, for HDP only, at the inlet height (Table 1) above the model's ground level (AGL). All of the WRF-driven STILT runs place the release point of air parcels following the AGL configuration. Error bars denote standard errors of the diurnal averages.

3 Results

3.1 Observed vs. simulated diurnal cycle

The observed and simulated diurnal cycles of CO_2 for the three selected RACCOON sites are shown in Fig. 3. These diurnal patterns were calculated from averaging the 3-hourly simulated time series from different model setups, which exhibit significant variability at multi-day synoptic timescales and correlations with different meteorological variables between HDP, SPL, and NWR (Fig. S5, Table S1). Due to this complexity we are focussing the analysis on the average diurnal pattern.

The observed diurnal cycle exhibits an amplitude of $\sim 2\,\mathrm{ppm}$, on average, with more elevated concentrations at night and depleted values during the day. In contrast to the observed diurnal cycles, the simulated CO_2 extracted from the site's altitude within CarbonTracker's output (Table 1) exhibits a different cycle. Instead of peaking at night, CO_2 in CarbonTracker reaches its maximum during the afternoon at HDP. At SPL and NWR, the diurnal cycle is significantly attenuated, with nighttime values barely elevated over the background instead of the nighttime enhancement in the observed values.

It appears that the erroneous diurnal pattern at HDP within CarbonTracker can partly be due to the diurnal reversal in the original biospheric fluxes, which showed strong uptake of CO_2 even at night for the grid cell where HDP is located (Fig. S2). This resulted in erroneous diurnal patterns at all of the lowest eight levels of CarbonTracker (Fig. S6), with the bottom two levels exhibiting strong depletions in CO_2 at night and enhancements during the day, pointing to unrealistic nighttime uptake and daytime release.

However, the diurnal reversal in biospheric fluxes alone does not completely explain the erroneous diurnal pattern. Differences in the diurnal pattern between GDAS–ASL simulations after introducing the diurnal fix in biospheric fluxes were not as pronounced at SPL and NWR.

The GDAS–ASL simulations show a pronounced peak of CO_2 in the morning that is missing from observations at all three sites (Fig. 3). We will discuss this feature, also seen in other coarse-scale simulations of mountaintop CO_2 (Geels et al., 2007), in Sect. 3.2 below.
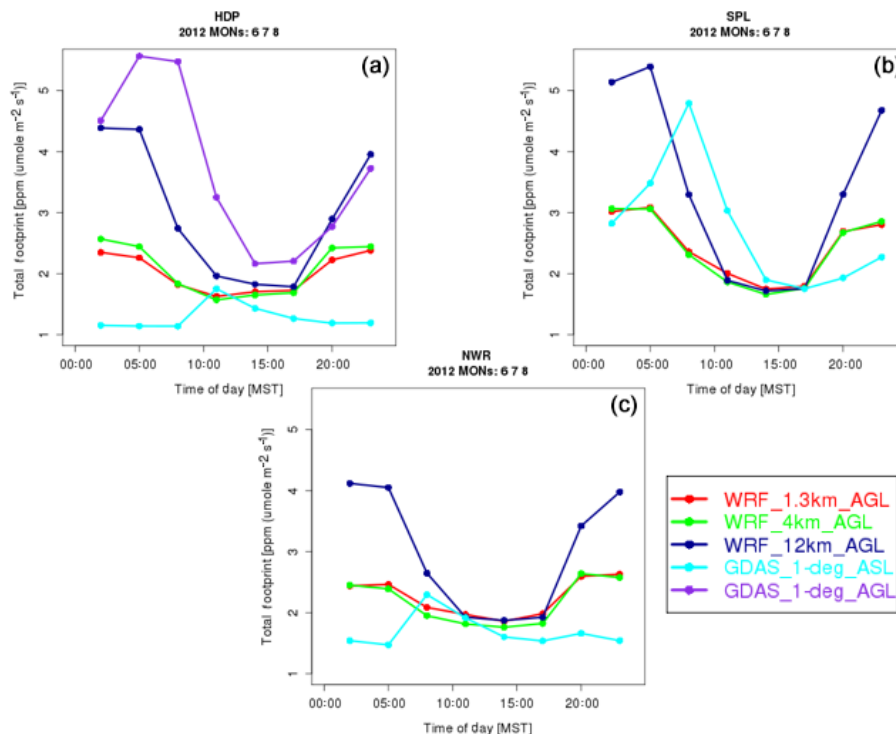
Figure 4. The average diurnal footprint strengths at HDP, SPL, and NWR over June–August 2012 from STILT, driven with different meteorological fields and release heights (ASL vs. AGL). The footprint strength was derived by summing over the spatial distribution of footprint values (Fig. 5).

In contrast to GDAS–ASL and CarbonTracker, the WRF-driven simulations better reproduce the shape of the observed diurnal cycle (Fig. 3), with nighttime enhancements and daytime depletions of CO_2. Considerable differences in nocturnal CO_2 concentrations are found, however, in the WRF–STILT runs at various grid spacings. WRF–12 km significantly overestimates CO_2 at night, while WRF–1.3 km and WRF–4 km produced similar CO_2 concentrations that correspond much more closely to observed values. While GDAS simulations started near the ground ("GDAS–AGL") also exhibit nighttime enhancements and daytime depletions of CO_2, the nighttime values are grossly estimated, exceeding even the values in WRF–12 km. Therefore, we do not present GDAS using the AGL configurations at the other two sites.

Part of the error in all the simulations against the observations could arise from errors in the CarbonTracker boundary condition imposed at the end of the STILT back trajectories. Evaluations of CT-2013b against aircraft vertical profiles (which were not assimilated into Carbon-Tracker) at the Trinidad Head and Estevan Point sites on the west coast of the North American continent carried out by the CarbonTracker team (http://www.esrl.noaa.gov/gmd/ccgg/carbontracker/CT2013B/profiles.php) indicate that CT-2013b overestimates CO_2 concentrations by at most 1.0 ppm, on average, during the summer season. Thus, the fact that

GDAS and CarbonTracker underestimate CO_2 at night likely cannot be attributed solely to a biased boundary condition.

3.2 Differences in simulated transport to mountaintop sites

3.2.1 Footprint patterns

In order to isolate the impact of differences in atmospheric transport on the simulated CO_2, we examine the average diurnal pattern of the footprint strength over Jun–Aug 2012 (Fig. 4). At each hour of the day we summed the spatially explicit map of the average footprint that marks out the source region of each RACCOON site – shown in Figs. 5–6 for HDP and in the Supplement for the other two sites. The result shows the diurnal pattern of the sensitivity of the receptor concentration to upwind fluxes.

To a large extent, the diurnal variation in footprint strength mirrors the simulated CO_2 concentrations. Nocturnal enhancements in the footprints are seen in the WRF-driven simulations, with the WRF–12 km exhibiting the strongest nocturnal footprints. Footprints from WRF–1.3 km and WRF–4 km are weaker at night than from WRF–12 km and closely resemble each other. GDAS–AGL footprints (only shown at HDP) are the highest among all models at night, leading to the drastic overestimation in CO_2 in Fig. 3. In contrast,
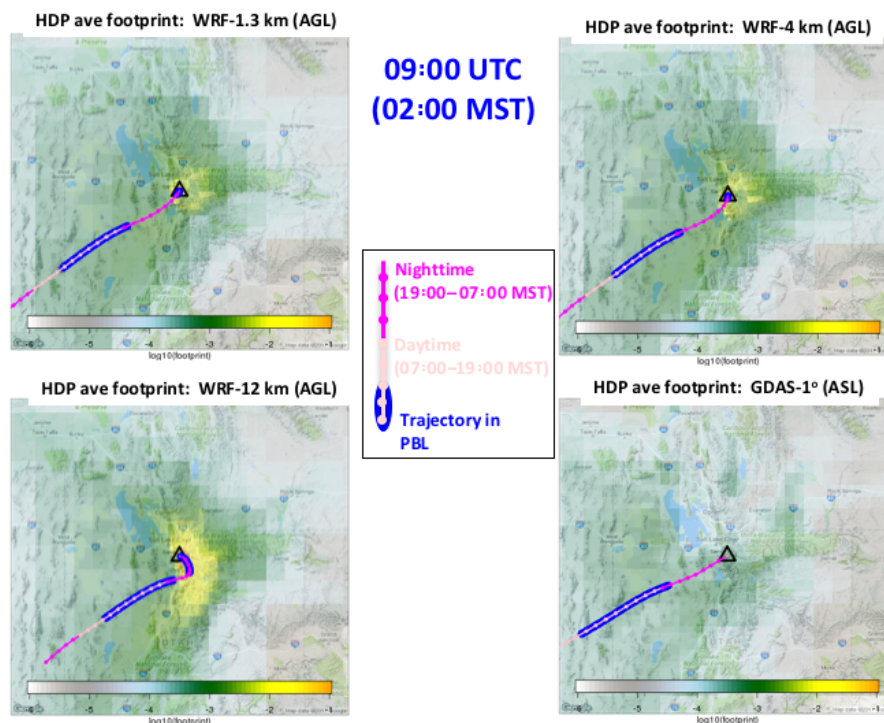
Figure 5. The average footprint (shown in log$_{10}$) for the Hidden Peak (HDP) site in Utah, at night: 02:00 MST (09:00 UTC), gridded at 0.1° × 0.1°. The site is denoted as a triangle. The average back trajectory (averaged over the stochastic STILT trajectories) is drawn as a line, with points indicating trajectory locations every hour, as the trajectory moves back from the site indicated as points. Magenta parts of the trajectory refer to the nighttime (19:00–07:00 MST), while pink portions indicate the daytime (07:00–19:00 MST). Parts of the trajectory are shaded with blue when it is found below the average height of the PBL along the trajectory.

GDAS–ASL footprints exhibit a peak in the morning and are generally smaller in value than their WRF counterparts at other times of the day at HDP and NWR. At SPL, the GDAS–ASL footprint strengths are stronger and more in line with values from the other models.

Footprints are weaker during the daytime, and in contrast to the nighttime, differences between footprint strengths simulated by different models are significantly smaller. In particular, the differences are minimized in the afternoon.

These patterns are also seen in the footprint maps. We further examine differences in the spatial patterns of average footprints produced from the various WRF and GDAS configurations. The spatial patterns are contrasted at two different times of the day, associated with the nighttime and afternoon hours: 02:00 MST (09:00 UTC) and 14:00 MST (21:00 UTC), respectively. Only HDP is shown for these 2 h of the day in Figs. 5 and 6; similar figures for SPL and NWR can be found in the Supplement (Figs. S7–S10). The footprint maps show marked differences at night (Fig. 5): the WRF–12 km footprints are clearly stronger than their counterparts from the other three model configurations, with higher values covering the Wasatch Range near the HDP site. Meanwhile, the GDAS–ASL footprint at 02:00 MST shows

a striking contrast, with very low values around HDP and the Wasatch area in general.

The afternoon footprints at 14:00 MST (Fig. 6) display much more similarity with each other. Not only do the spatial patterns between the WRF and GDAS runs resemble one another; the significant differences in footprint strengths, with overestimation by WRF–12 km and underestimation by GDAS–ASL, are no longer found. The aforementioned nighttime divergence and afternoon correspondence between footprint patterns are repeated at the SPL and NWR sites (Figs. S7–S10).

To further understand the nighttime divergence between model configurations, we now examine the average air parcel trajectories within Figs. 5 and 6. It is worth noting that these trajectories differ from conventional mean wind trajectories that do not incorporate effects from turbulent dispersion (Lin, 2012). Instead, these mean trajectories are determined by averaging the 2000 stochastic air parcel trajectories from STILT used for simulating transport arriving at a specific hour at a particular site and then averaging over the ∼ 90 days spanning June–August 2012. Thus, there are ∼ 180 000 stochastic trajectories averaged into generating the mean trajectory, thereby incorporating the net effect of turbulence on atmospheric transport. An example showing a
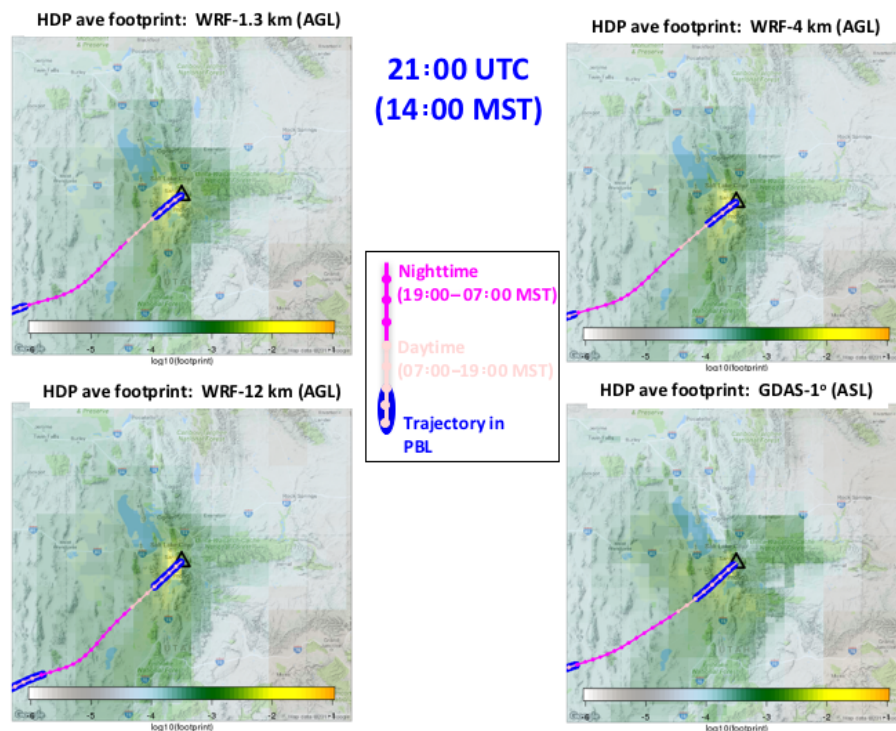
Figure 6. Similar to Fig. 5, but for the afternoon: 14:00 MST (21:00 UTC) at HDP.

subset of stochastic air parcels giving rise to the average trajectory is given in Fig. S1 for NWR, for 14:00 MST.

Similar to the footprints, average trajectories differ much more at night than in the afternoon. Differences in average air parcel trajectories and the underlying resolved mountainous terrain are further examined in the next section.

3.2.2 Three-dimensional terrain and trajectories

The 3-D terrain plots in Figs. 7, 9, and 11 illustrate the degradation in terrain resolved by coarser grid spacings and the resulting differences in average STILT-derived stochastic air parcel trajectories started at night (09:00 UTC) from the three sites. The afternoon (21:00 UTC) plots are shown in the Supplement (Figs. S11–S13). The PBL heights, which determine whether air parcels are affected by surface fluxes (and lead to nonzero footprint values), are also plotted as blue lines in the same plots. Note that the apparent intersection of the PBL height with the ground in Figs. 7 and 9 is an artifact from the averaging of multiple PBL heights along stochastic trajectories (Fig. S1).

Despite terrain smoothing compared against WRF–1.3 km, WRF–4 km produced STILT trajectories that are very similar to those from WRF–1.3 km at all three sites, suggesting that salient features of the mountain flows resolved with 1.3 km spacing are also found in the 4 km spacing. In contrast, WRF–12 km and GDAS–ASL both differed significantly from the more finely gridded WRF simulations. Not

only did the trajectories deviate from the higher resolution counterparts, but the relationships between the trajectory vis-à-vis the PBL height, critical for determining footprints and simulating CO_2 changes (Sect. 2.2), also differ. The WRF–12 km trajectories spend more time within the PBL, while GDAS–ASL trajectories are found much less within the PBL, because they start at a greater height above ground level.

An alternative perspective is to view the trajectory and PBL heights relative to the ground surface (AGL) instead of above sea level, at each time step backward in time from the receptor (Figs. 8, 10, and 12). These figures highlight the fact that while PBL dynamics in the three WRF configurations are similar, the heights of the trajectories relative to the PBL height differ. The trajectory exits above the nocturnal PBL 1 h backward in time, on average, while the WRF–12 km trajectory spends several hours within the PBL.

The difference in the trajectory behavior can be explained by the differing terrain. In mountainous terrain, PBL heights generally follow the terrain elevations, albeit with attenuated amplitude (Steyn et al., 2013). Thus, in WRF–1.3 km and 4 km, the more highly resolved terrain produced shallow nocturnal PBL heights that descend in the valley (Fig. 7) while the corresponding trajectory hovers above it. Viewed relative to the ground surface (Fig. 8), the trajectory originating from HDP appears to have exited above the nocturnal PBL in WRF–1.3 km and 4 km. In contrast, due to the significantly "flattened" mountains in WRF–12 km and in GDAS, the PBL heights exhibit less spatial variation near the moun-
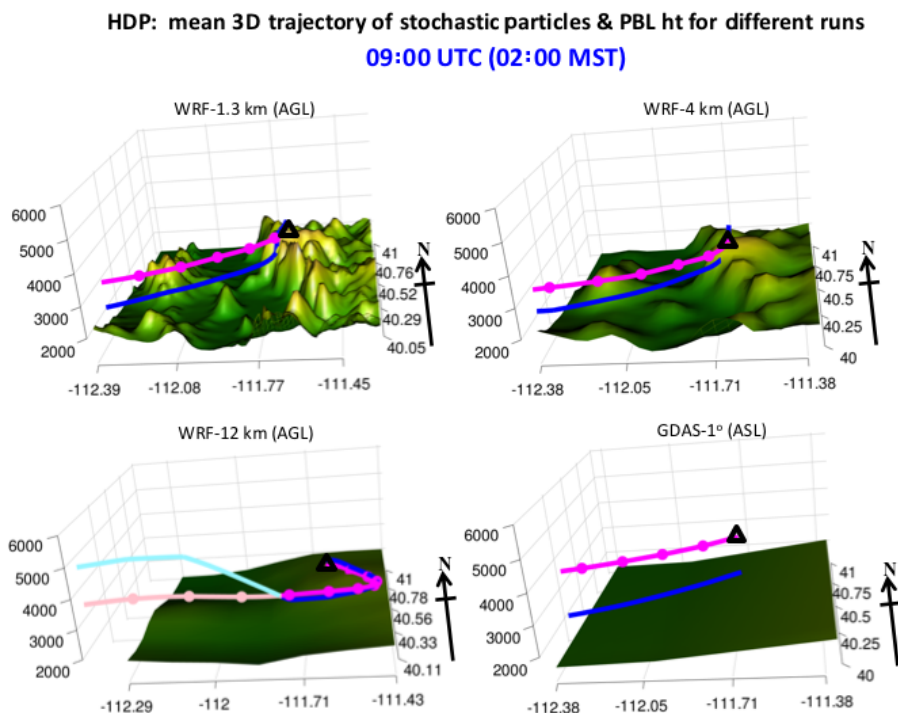
Figure 7. Three dimensional plots of the terrain over a domain of $\sim 1° \times 1°$ surrounding HDP, as resolved by the WRF and GDAS models at various grid spacings. The HDP site is denoted as a triangle. Also shown is the average back trajectory, derived by averaging locations of the numerous stochastic trajectories simulated by STILT, driven by the various WRF meteorological fields and the global GDAS field. Back trajectories were started from HDP at 02:00 MST (09:00 UTC). Points indicate trajectory locations every hour, as the trajectory moves back from the site indicated as points. Magenta portions of the trajectory refer to the nighttime (19:00–07:00 MST), while pink portions indicate the daytime (07:00–19:00 MST). In addition, the PBL heights averaged along the back trajectory are shown as the blue line.

taintop receptor, since the terrain itself was smoothed. Consequently, WRF–12 km trajectories, unlike the WRF–1.3 km or 4 km cases, travel closer to the ground surface, within the nighttime PBL, even as it is advected away from the three RACCOON sites (Figs. 7 and 8). This resulted in stronger nighttime footprints in WRF–12 km as seen in Figs. 4 and 5. Another effect of the proximity of the air parcels to the model's ground surface is the slower wind speeds from surface drag, causing the air parcel trajectories to remain close to the three sites until the previous day; for HDP and SPL, the mean trajectories spiral toward the site at the surface, following an "Ekman wind spiral" pattern (Holton, 1992). In WRF–1.3 km and WRF–4 km, the measurement sites are at significantly higher elevations above the resolved valleys in the area surrounding the sites, and the air parcels are found above the shallow nocturnal boundary layer hugging the valley floor, on average (Fig. 7).

Although both WRF–12 km and GDAS poorly resolve the mountains, a key difference in the case of GDAS–ASL is that the air parcels were released at a site's elevation above sea level (following what is generally done in CarbonTracker and other global models), much higher above ground than the release used in WRF–12 km, which was selected to be the height in AGL above the flattened mountain. Therefore, the

GDAS–ASL trajectories were significantly higher than the PBL height in the model (particularly at HDP and NWR), which followed the flattened ground surface in the $1° \times 1°$ grid spacing. Another noticeable difference in the GDAS–ASL trajectory was the significantly higher daytime PBL heights (Figs. 8, 10, and 12). We suspect this is because of the greatly reduced vertical resolution within GDAS (23 levels vs. 41 levels in WRF), since STILT diagnoses the PBL height to correspond to a model level, a higher PBL height was chosen for GDAS because of the thicker vertical level. Another subtle artifact of the coarse resolution within GDAS can be seen in the anomalously low daytime PBL height just in the vicinity of HDP (Figs. 13 and S11). It appears that the GDAS model set an entire $1° \times 1°$ grid box near HDP to be the water body (the Great Salt Lake), thereby suppressing the PBL height.

The three-dimensional plots can explain the higher nighttime footprint strengths at SPL (Figs. 4 and S7). This result appears to be a consequence of the relative elevation of the site and surrounding terrain. The elevation of the surrounding valley floor at SPL is closer to that of the mountaintop location of SPL (Fig. 9); therefore, air parcels released from SPL would have a stronger tendency to reside within the PBL even over the surrounding valleys, unlike the steeper drop-
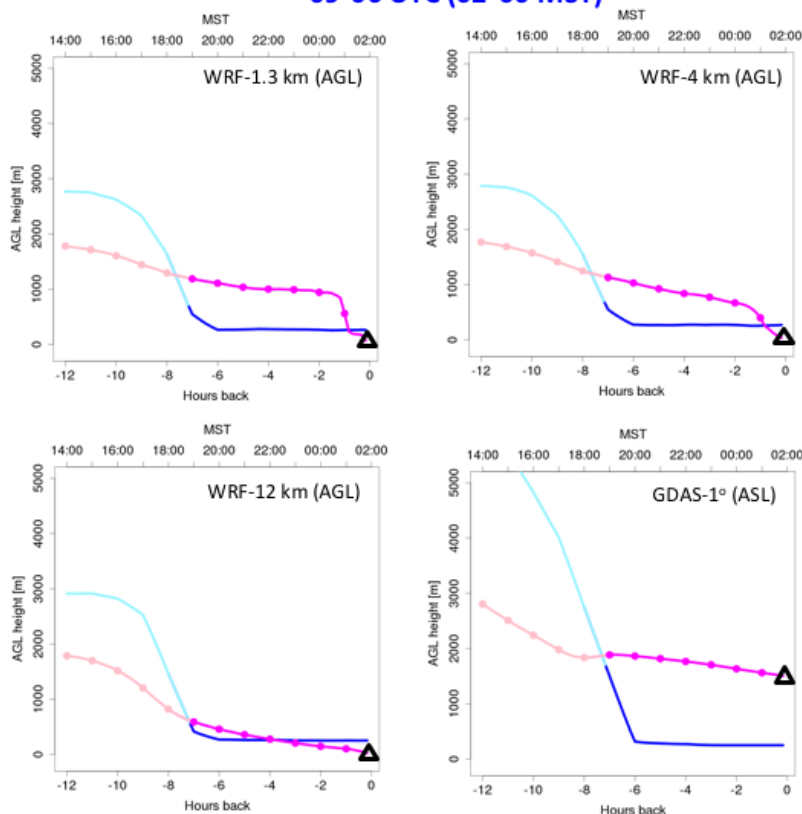
Figure 8. Time series of the average back trajectory and PBL heights relative to the ground surface (AGL) instead of above sea level, at each time step backward in time from the receptor (triangle). Magenta portions of the trajectory refer to the nighttime (19:00–07:00 MST), while pink portions indicate the daytime (07:00–19:00 MST). The PBL heights averaged along the back trajectory are shown as the blue line. The nighttime PBL height is indicated in dark blue, while the daytime portion is in light blue. The height of the site is indicated by the black triangle at the starting time of the back trajectory.

off – i.e., deeper valley – upwind of HDP (Fig. 7) and NWR (Fig. 11).

As already found in the footprints (Fig. 5), the afternoon (21:00 UTC) differences in air parcel trajectories are much smaller (Figs. S11–S13). We suspect that this is due to the fact that the deeper daytime PBL height causes the trajectories to reside within the PBL, and stronger mixing within the daytime PBL minimize the relative terrain differences. A previous modeling study focusing on the SPL area has also suggested the daytime afternoon PBL depth to extend above the mountaintop (De Wekker et al., 2009), indicating that differences between terrain resolution and the resulting flows could be reduced due to the strong mixing taking place within the deep afternoon PBL. Consequently, simulations in the afternoon show much smaller divergence between various model configurations, resulting in similar footprint strengths and CO$_2$ values (Figs. 3 and 4). More evidence of the convergence in afternoon simulated CO$_2$ can be found in the small differences in CO$_2$ modeled at CarbonTracker's different levels during this time (Fig. S6).

A few studies have specifically focused on the flows and atmospheric transport around the NWR site. These authors have pointed to thermally driven flows, particularly downs-lope drainage flow events at night (Sun et al., 2007; Sun and De Wekker, 2011; Blanken et al., 2009). Daytime upslope events, while weaker, were also noted (Sun and De Wekker, 2011; Blanken et al., 2009; Parrish et al., 1990). It may seem that the 3-D trajectories in Figs. 11 and S13 run counter to the presence of such thermally driven flows. We suspect that this is because the thermally driven flows induced by the terrain cannot be discerned in the mean trajectories, which also reflect the larger-scale flows that can be stronger than the local scale thermally driven flows (Zardi and Whiteman, 2013). When one examines the stochastic trajectories from which the mean trajectories are based (Fig. S1), it is clear that some upslope trajectories can be detected.

We now examine the reason for the erroneous daytime peak in simulated CO$_2$ from GDAS–ASL that does not show up in the observations (Fig. 3). We specifically focus on this feature because the daytime peak was also found
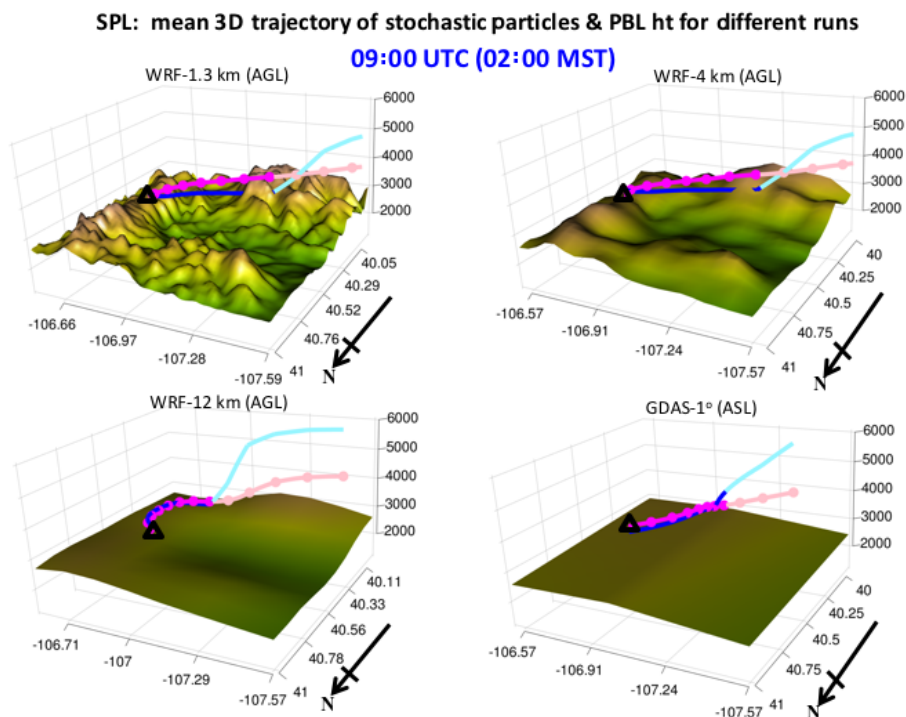
Figure 9. Similar to Fig. 7, but for the Storm Peak Laboratory (SPL) site.

in other coarse-scale simulations of CO_2 for mountaintop sites – e.g., in Europe (Geels et al., 2007). Focusing on the three-dimensional plots at the hours of 08:00 and 11:00 MST (Fig. 13), when the simulated peaks are found at SPL and both NWR and HDP, respectively, the peaks coincide with times when average trajectories are found within a relatively shallow morning PBL. As the air parcels move backward in time, when the morning transitions backward in time to the nighttime, many of them would still be found within the shallow nighttime PBL. Due to the shallowness of the nocturnal PBL, the footprint values for the air parcels found there would be high. These parcels would also be sampling the nighttime CO_2 release and therefore lead to enhancements in CO_2. In other words, the erroneous daytime peak reflects enhanced CO_2 that is vented up to the observing height within the model during the day. We suspect that something similar is taking place in other global models, leading to similar erroneous daytime CO_2 peaks (Geels et al., 2007).

4 Discussion

This study has sought to answer the question: how can mountaintop CO_2 observations be used to constrain regional-scale carbon fluxes, given the complex terrain and flows in the vicinity of mountaintop sites? To address this question, we have driven a Lagrangian particle dispersion model simulating the transport of turbulent air parcels arriving at three mountaintop CO_2 sites in the western US. We then examined

potential differences in simulated results as the atmospheric simulations are driven by meteorological fields resolved with differing grid spacings and at different vertical levels.

We found that the observed average diurnal CO_2 pattern is better reproduced by simulations driven by WRF–1.3 km and WRF–4 km (AGL configuration), with minimal differences between the two configurations (Fig. 3). The coarser-scale models (WRF–12 km_AGL, GDAS-1°, and CarbonTracker) fail to reproduce the observed diurnal pattern at all three sites. The problem is especially severe at night, when both GDAS–ASL and CarbonTracker lack the nocturnal enhancements. In contrast, WRF–12 km (AGL) shows nocturnal CO_2 buildup that is clearly too strong. The overestimation problem is exacerbated when both coarser grid spacing and AGL configuration are adopted, as seen in GDAS–AGL at HDP (Fig. 3).

The overestimate in nighttime CO_2 from WRF–12 km (AGL) is due to the preponderance of simulated air parcels found within the nocturnal PBL (Figs. 7–9), which can be traced to the fact that air parcels are closer to the ground surface when mountains are flattened. Conversely, when released at ASL levels air parcels are found much higher above the nocturnal PBL due to the flattening of mountains in a coarse-scale global model like GDAS, resulting in minimal sensitivity to nighttime biospheric fluxes and a lack of CO_2 buildup. Such large errors in estimated carbon fluxes due to lack of ability to resolve patterns have also been found in earlier studies in Europe (Pillai et al., 2011; Peters et al., 2010).
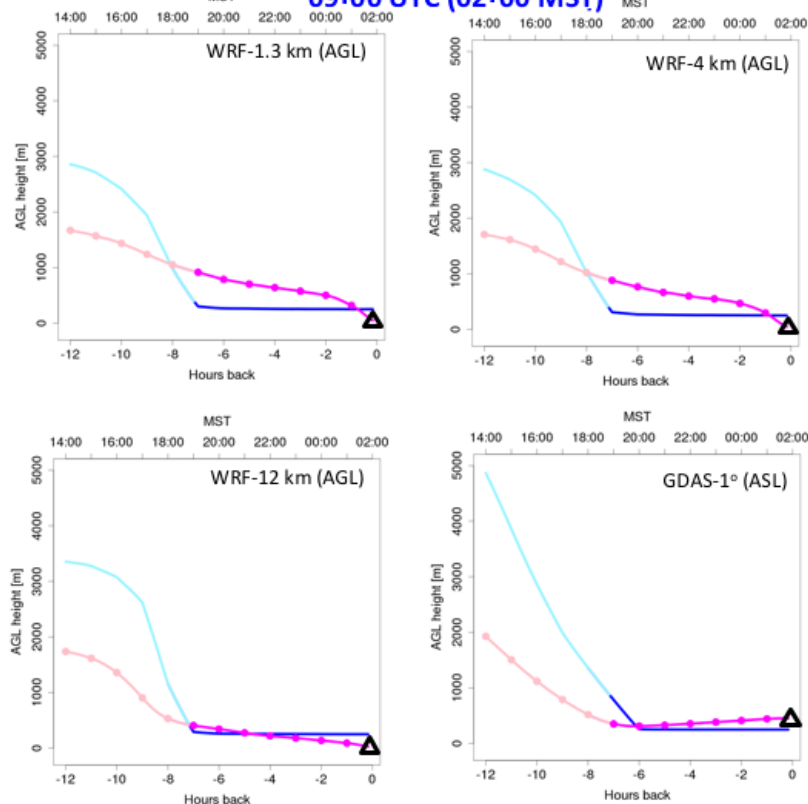
Figure 10. Similar to Fig. 8, but for the Storm Peak Laboratory (SPL) site.

The natural question, then, is what can researchers do with mountaintop CO$_2$ observations, given the difficulty in resolving the terrain and flows in complex terrain?

4.1 Approach 1: adjust vertical level of simulations from which to compare against observed values

The diurnal cycle simulated within CarbonTracker varies significantly as a function of the vertical level (Fig. S6) from which CO$_2$ is extracted, particularly at night. The strongly attenuated diurnal cycle in the interpolated level corresponding to the ASL elevation of the mountaintop sites (orange dashed) is found at higher levels within CarbonTracker too, away from the first few levels near the ground. At HDP, the nighttime depletion of CO$_2$ at lower levels appears to be due to the erroneous nighttime photosynthetic uptake in the grid cell where HDP is located (Fig. S2).

Interestingly, at SPL and NWR the diurnal pattern at a level between levels 2 and 3 appears to correspond more closely to the overall observed CO$_2$ diurnal cycle, perhaps due to the presence of nighttime enhancements closer to the model surface that is absent from the higher levels closer to the ASL elevation. The closer correspondence to observed patterns may call for researchers to adjust the vertical level

to maximize resemblance to observations. This was carried out at Jungfraujoch (Folini et al., 2008), where the authors simulated carbon monoxide (CO) at multiple heights and arrived at a height of 80 m above the model's ground surface as the best correspondence with the observed CO, which was measured closer to the ground (Rinsland et al., 2000). Instead, a different study simulating observations at the same site adopted a height of 830 m above the model ground surface (Tuzson et al., 2011). This example illustrates the divergence in researchers' choices for the vertical level in the midst of mountainous terrain.

It is worth noting that the introduction of additional degrees of freedom in the vertical level in "fitting" the measured CO$_2$ diurnal cycle within a carbon assimilation system is potentially problematic. The reason is that the assimilation system seeks to solve for carbon fluxes by examining the mismatch between observed vs. simulated CO$_2$ concentrations. If the mismatch is due to erroneous fluxes, the introduction of additional degrees of freedom in the vertical level would compensate for erroneous fluxes. For instance, if the nighttime carbon fluxes are overestimated in the model, this should show up as an enhanced CO$_2$ concentration that is larger than observed values. However, this overestimation in CO$_2$ would be reduced by picking a higher vertical level
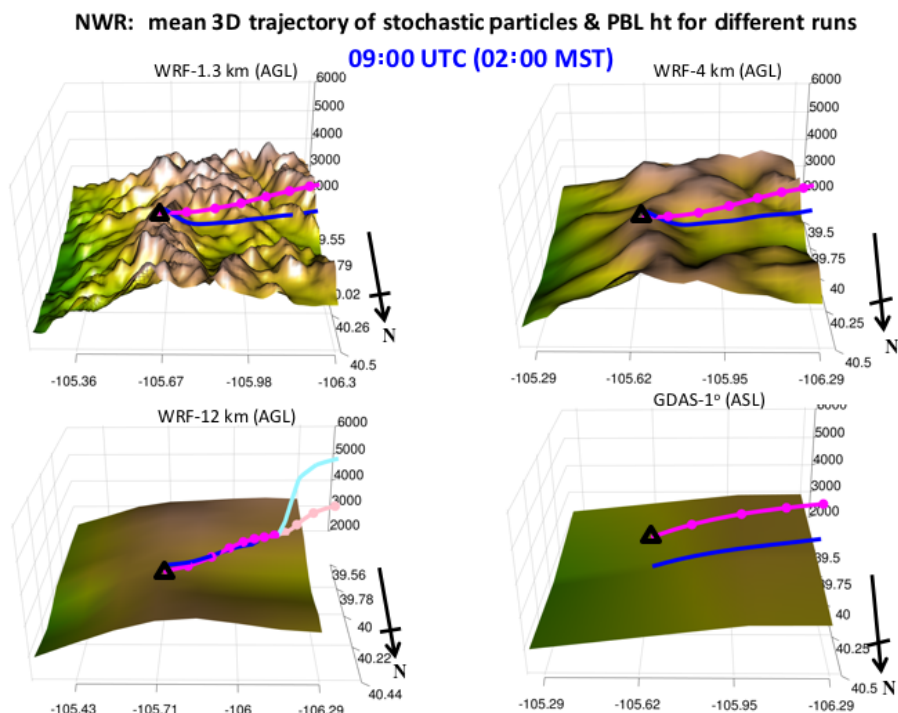
Figure 11. Similar to Fig. 9, but for the Niwot Ridge (NWR) site.

rather than fixing the overly large efflux in the model. The optimal level could differ between night and day as well; for instance, a level higher than Level 2 would fit better against observations during the daytime at SPL and NWR (Fig. S6). If different levels were adopted at different times of the day, the degrees of freedom that can be adjusted would be even larger, and model–data mismatches would be used in vertical level adjustments instead of correcting erroneous biospheric fluxes.

Regardless, there is some role for vertical level adjustments to remove the gross mismatch in the observed vs. simulated diurnal cycles. If the vertical level is indeed adjusted in a carbon inversion system, we suggest that additional information (e.g., comparisons to meteorological observations or other tracers) is used rather than maximizing the match to the target species (i.e., CO_2, in the case of a carbon inversion system).

The CO_2 values at multiple levels within CarbonTracker show that unlike the nighttime, differences between vertical levels are much smaller during the afternoon at SPL and NWR (Fig. S6), suggesting that the simulated CO_2 values are not as sensitive to the choice of vertical level. We suspect that the large differences between vertical levels at HDP are due to the flipped diurnal cycle in biospheric fluxes within CarbonTracker (Fig. S3). Otherwise, the lack of sensitivity to the choice of vertical level suggests that coarse-scale models should assimilate afternoon observations, rather than nighttime observations (see "Approach 3" below).

4.2 Approach 2: assign errors to account for model errors

Instead of neglecting the mountaintop CO_2 observations altogether, an alternative approach is to make use of the observations, but to assign them errors within the model–measurement discrepancy error covariance matrix to account for model deficiencies (Lin and Gerbig, 2005; Gerbig et al., 2008). One estimate of the model–measurement discrepancy error is the root-mean-square error (RMSE), which ranges from less than 3 ppm for WRF–1.3 km to over 7 ppm for WRF–12 km (Fig. S5). In this way, the inversion system would assign less weight to observations that the model has difficulties simulating. Given the systematic misrepresentation of the diurnal cycle in coarse-scale models, particularly at night (Fig. 3), this approach will effectively throw away much of the data as noise, due to inadequacies in the model. This naturally leads to the next possible approach of just having coarse-scale models assimilate afternoon observations.

4.3 Approach 3: have coarse-scale models assimilate afternoon observations instead of nighttime

Our results show that the simulated CO_2 values are more in accordance with observed values in the afternoon (Fig. 3). This follows from the fact that afternoon trajectories and footprints match their higher resolution counterparts (Figs. 6, S8, and S10–S13), likely due to the deeper afternoon PBL depth and the reduction of terrain effects (Steyn et al., 2013).
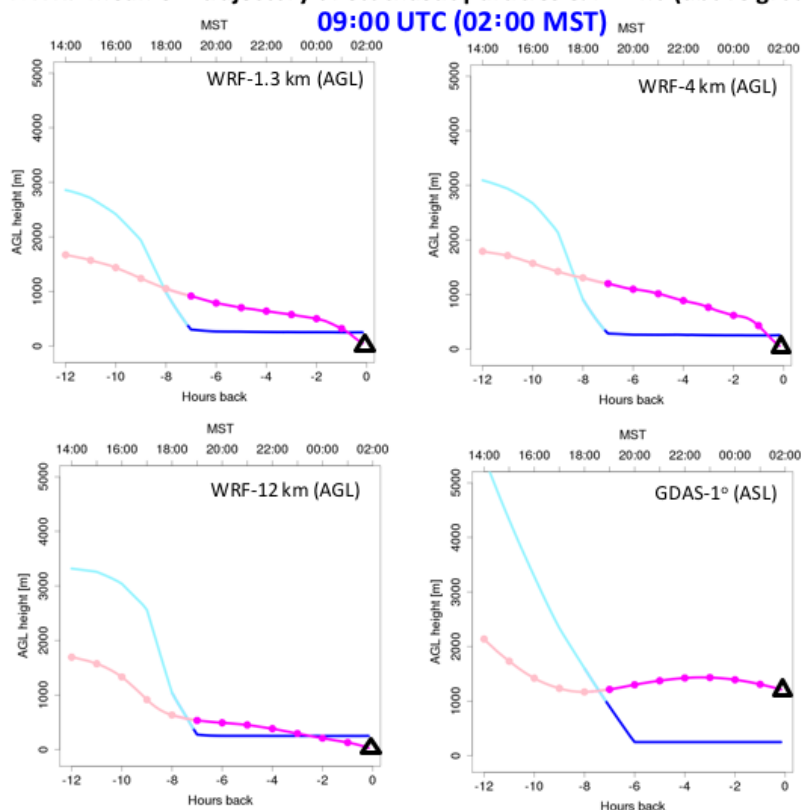
Figure 12. Similar to Fig. 10, but for the Niwot Ridge (NWR) site.

In other words, relative differences in PBL depth associated with flattening of mountains are lessened when the PBL is deeper; thus, the impact on whether an air parcel sampled by the mountaintop site falls within the PBL is also attenuated under afternoon vigorous mixing conditions.

Based on these results, and in lieu of better transport, we suggest coarse-scale models may be better served to assimilate afternoon observations over the continent at their above sea level elevation. This is contrary to what has been commonly practiced by researchers, when nighttime mountaintop observations were assimilated (Peters et al., 2007; Keeling et al., 1976) to avoid daytime upslope flows and when nocturnal observations that represent free-tropospheric conditions would better match coarse resolution models. We have found that sampling coarse-scale (1°) models at the corresponding ASL height has significant difficulties simulating nighttime CO$_2$, since it appears that the model failed to represent the strength of the nocturnal footprint at the three RACCOON mountaintop sites (Figs. 4 and 5). Thus, the inability of coarse-scale models to simulate the transport and PBL depths results in the lack of nocturnal enhancements and thereby the wrong diurnal cycle (Fig. 3). Conversely, sampling the 12 km simulation at the AGL height also has significant difficulties simulating nighttime CO$_2$, because it overestimates the nocturnal footprint.

However, careful attention needs to be paid to upslope flows in the afternoon and the potential misinterpretation of more localized biospheric signals or anthropogenic signals from below the mountain. A study from Jungfraujoch in Europe suggested that as much as $\sim 40\%$ of the days in a year are influenced by thermally driven flows (Griffiths et al., 2014). During the afternoon, the mountaintop site would then be influenced by thermally driven upslope winds, as also pointed out by a number of studies around NWR, along the Colorado Front Range (Sun et al., 2010; Sun and De Wekker, 2011; Parrish et al., 1990) as well as SPL (De Wekker et al., 2009). For sites like HDP and NWR, which have large nearby urban areas at lower elevation, upslope conditions can be of particular concern if not properly accounted for. If these sites experience elevated CO$_2$ in the afternoon from pollution sources, and this transport is not captured by the models, then natural CO$_2$ sources can be significantly overestimated.

We found it encouraging that despite the proximity of significant population and anthropogenic emissions from the Salt Lake and Denver area to the HDP and NWR sites, respectively, the WRF–1.3 km model suggests that the additional contribution of anthropogenic CO$_2$ in the afternoon, over and beyond the nighttime signal, is less than 1 ppm, on average (Fig. S4). Presumably this is because of the high elevation of HDP and NWR in relation to the urban area and the
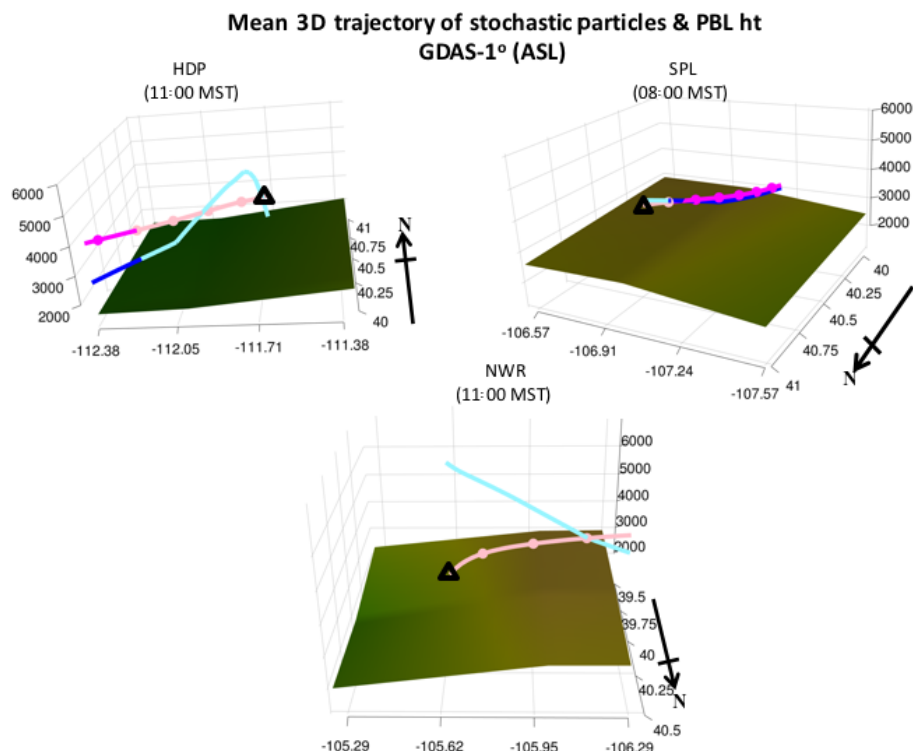
Figure 13. Similar to three-dimensional terrain and trajectory plots as shown in Figs. 7, 9, and 11, but for just the GDAS 1°. ASL simulations and for the morning hours of 08:00 and 11:00 MST.

dilution of signals as they move upslope; the afternoon urban signal would be enhanced if the sites were placed at lower peaks.

Regardless, it is prudent to consider mountaintop sites as not necessarily "pristine" sites and to consider potential contributions from surrounding anthropogenic emissions on these observations. It has been estimated that as of the year 2000, over 10 % of the world population lives in mountainous areas (Huddleston et al., 2003), meaning that any mountaintop site could very well see anthropogenic signatures. We recommend additional tracers to be measured in conjunction with the mountaintop CO$_2$ sites. For instance, combustion tracers such as ^{14}C and CO (Levin and Karstens, 2007) have been measured alongside CO$_2$ at mountaintop sites in Europe. Another promising tracer is ^{222}Rn (Griffiths et al., 2014), which provides a measure of surface exchange and would help provide constraints on the exchange of air measured at the mountaintop with the surface. Co-located meteorological observations – whether in situ or remotely sensed (e.g., radar, sodar, or lidar) – to probe atmospheric flows and turbulent mixing would also be of significant value in helping to interpret the tracer observations (Rotach et al., 2014; Banta et al., 2013).

4.4 Approach 4: adopt high-resolution modeling frameworks

The least problematic, though potentially costly in terms of computational time, approach to reduce modeling errors when interpreting mountaintop CO$_2$ observations is to adopt a high resolution modeling framework. This conclusion was also arrived at by previous studies (Pillai et al., 2011; van der Molen and Dolman, 2007; De Wekker et al., 2009). From our results, it appears that meteorological fields from WRF at 4 km grid spacing, driving a Lagrangian particle dispersion model, can reproduce most features from a 1.3 km simulation and generate a CO$_2$ diurnal cycle that qualitatively matches the observed pattern. Once the WRF fields are degraded to 12 km grid spacing, the model fails to capture such features.

While at least 4 km resolution in the meteorological fields is needed for the sites examined here in the American Rockies, we anticipate that the minimum resolution would depend on the level of complexity in the terrain, the height of the observational site, and relationship with surrounding sources/sinks.

5   Conclusions

Given the large extent of the Earth's surface covered by hills and mountains and the large amount of biomass and potential for carbon storage in complex terrain (Fig. 1), we call for expanded efforts in observing and modeling CO_2 and other tracers on mountaintop sites. This study has illustrated the potential for even coarse-scale models to extract information from these observations when focusing on the daytime and afternoon values and the ability of high resolution models to simulate the general features of the summertime diurnal CO_2 cycle even in the midst of significant terrain complexity. However, we acknowledge that even the highest-resolution model adopted in this paper undoubtedly is subject to limitations of its own and that deviations between simulated vs. observed CO_2 diurnal cycles arise from errors in both atmospheric transport as well as the biospheric fluxes. Due to the focus on atmospheric transport in this paper, errors in the simulations caused by shortcomings in the biospheric fluxes remain outside the scope of this study (except for corrections to the flipped diurnal cycle; Fig. S3)

Even though current models remain imperfect, we call for sustained and expanded observations of CO_2 and other tracers (e.g., CO, ^{222}Rn, and the isotopes of CO_2) co-located with meteorological observations on mountaintop sites to create enhanced datasets that can be further utilized by modeling frameworks of the future. Finally, we call for testing and gathering of three-dimensional CO_2 observations over complex terrain, as revealed by intensive airborne campaigns like the Airborne Carbon in the Mountains Experiment (Sun et al., 2010).

Data availability.   All of the simulation output used in this paper can be accessed at http://lair.utah.edu/page/project/biomass/about/.

The Supplement related to this article is available online at doi:10.5194/acp-17-5561-2017-supplement.

Competing interests.   The authors declare that they have no conflict of interest.

Edited by: R. Cohen
Reviewed by: three anonymous referees

References

Anderegg, W. R. L., Berry, J. A., Smith, D. D., Sperry, J. S., Anderegg, L. D. L., and Field, C. B.: The roles of hydraulic and carbon stress in a widespread climate-induced forest die-off, P. Natl. Acad. Sci., 109, 233–237, doi:10.1073/pnas.1107891109, 2012.

Arora, V. K., Boer, G. J., Friedlingstein, P., Eby, M., Jones, C. D., Christian, J. R., Bonan, G., Bopp, L., Brovkin, V., Cadule, P., Hajima, T., Ilyina, T., Lindsay, K., Tjiputra, J. F., and Wu, T.: Carbon–Concentration and Carbon–Climate Feedbacks in CMIP5 Earth System Models, J. Climate, 26, 5289–5314, doi:10.1175/jcli-d-12-00494.1, 2013.

Bakwin, P. S., Tans, P. P., Hurst, D. F., and Zhao, C.: Measurements of carbon dioxide on very tall towers: results of the NOAA/CMDL program, Tellus B, 50, 401–415, 1998.

Baldocchi, D., Falge, E., Gu, L., Olson, R., Hollinger, D., Running, S., Anthoni, P., Bernhofer, C., Davis, K., Evans, R., Fuentes, J., Goldstein, A., Katul, G., Law, B., Lee, X., Malhi, Y., Meyers, T., Munger, W., Oechel, W., Paw U, K. T., Pilegaard, K., Schmid, H. P., Valentini, R., Verma, S., Vesala, T., Wilson, K., and Wofsy, S.: FLUXNET: A new tool to study the temporal and spatial variability of ecosystem-scale carbon dioxide, water vapor and energy flux densities, B. Am. Meteorol. Soc., 82, 2415–2435, 2001.

Banta, R. M., Shun, C. M., Law, D. C., Brown, W., Reinking, R. F., Hardesty, R. M., Senff, C. J., Brewer, W. A., Post, M. J., and Darby, L. S.: Observational Techniques: Sampling the Mountain Atmosphere, in: Mountain Weather Research and Forecasting: Recent Progress and Current Challenges, edited by: Chow, K. F., De Wekker, F. J. S., and Snyder, J. B., Springer Netherlands, Dordrecht, 409–530, 2013.

Blanken, P. D., Williams, M. W., Burns, S. P., Monson, R. K., Knowles, J., Chowanski, K., and Ackerman, T.: A comparison of water and carbon dioxide exchange at a windy alpine tundra and subalpine forest site near Niwot Ridge, Colorado, Biogeochemistry, 95, 61–76, doi:10.1007/s10533-009-9325-9, 2009.

Blyth, S., Groombridge, B., Lysenko, I., Miles, L., and Newton, A.: Mountain Watch: Environmental Change and Sustainable Development in Mountains, UNEP World Conservation Monitoring Centre, 2002.

Brooks, B.-G. J., Desai, A. R., Stephens, B. B., Bowling, D. R., Burns, S. P., Watt, A. S., Heck, S. L., and Sweeney, C.: Assessing filtering of mountaintop CO_2 mole fractions for application to inverse models of biosphere-atmosphere carbon exchange, Atmos. Chem. Phys., 12, 2099–2115, doi:10.5194/acp-12-2099-2012, 2012.

Brooks, B.-G. J., Desai, A. R., Stephens, B. B., Michalak, A. M., and Zscheischler, J.: Feasibility for detection of ecosystem response to disturbance by atmospheric carbon dioxide, Biogesciences Discuss., doi:10.5194/bg-2016-223, 2016.

Cox, P. M., Betts, R. A., Jones, C. D., Spall, S. A., and Totterdell, I. J.: Acceleration of global warming due to carbon-cycle feedbacks in a coupled climate model, Nature, 408, 184–187, 2000.

De Wekker, S. F. J., Ameen, A., Song, G., Stephens, B. B., Hallar, A. G., and McCubbin, I. B.: A Preliminary Investigation of

Boundary Layer Effects on Daytime Atmospheric CO$_2$ Concentrations at a Mountaintop Location in the Rocky Mountains, Acta Geophys., 57, 904–922, 2009.

Denning, A. S., Randall, D. A., Collatz, G. J., and Sellers, P. J.: Simulations of terrestrial carbon metabolism and atmospheric CO$_2$ in a general circulation model, Part 2: Simulated CO$_2$ concentrations, Tellus B, 48, 543–567, 1996.

Desai, A. R., Moore, D. J. P., Ahue, W. K. M., Wilkes, P. T. V., De Wekker, S. F. J., Brooks, B.-G., Campos, T., Stephens, B. B., Monson, R. K., Burns, S. P., Quaife, T., Aulenbach, S. M., and Schimel, D. S.: Seasonal pattern of regional carbon balance in the central Rocky Mountains from surface and airborne measurements, J. Geophys. Res.-Biogeo., 116, G04009, doi:10.1029/2011JG001655, 2011.

European Commission: Joint Research Centre/Netherlands Environmental Assessment Agency, Emission Database for Global Atmospheric Research (EDGAR), Release version 4.0, 2009.

Fisher, J. B., Sikka, M., Oechel, W. C., Huntzinger, D. N., Melton, J. R., Koven, C. D., Ahlström, A., Arain, M. A., Baker, I., Chen, J. M., Ciais, P., Davidson, C., Dietze, M., El-Masri, B., Hayes, D., Huntingford, C., Jain, A. K., Levy, P. E., Lomas, M. R., Poulter, B., Price, D., Sahoo, A. K., Schaefer, K., Tian, H., Tomelleri, E., Verbeeck, H., Viovy, N., Wania, R., Zeng, N., and Miller, C. E.: Carbon cycle uncertainty in the Alaskan Arctic, Biogeosciences, 11, 4271–4288, doi:10.5194/bg-11-4271-2014, 2014.

Folini, D., Ubl, S., and Kaufmann, P.: Lagrangian particle dispersion modeling for the high Alpine site Jungfraujoch, J. Geophys. Res.-Atmos., 113, D18111, doi:10.1029/2007JD009558, 2008.

Friedlingstein, P., Dufresne, J. L., Cox, P. M., and Rayner, P.: How positive is the feedback between climate change and the carbon cycle?, Tellus B, 55, 692–700, 2003.

Geels, C., Gloor, M., Ciais, P., Bousquet, P., Peylin, P., Vermeulen, A. T., Dargaville, R., Aalto, T., Brandt, J., Christensen, J. H., Frohn, L. M., Haszpra, L., Karstens, U., Rödenbeck, C., Ramonet, M., Carboni, G., and Santaguida, R.: Comparing atmospheric transport models for future regional inversions over Europe – Part 1: mapping the atmospheric CO$_2$ signals, Atmos. Chem. Phys., 7, 3461–3479, doi:10.5194/acp-7-3461-2007, 2007.

Gerbig, C., Körner, S., and Lin, J. C.: Vertical mixing in atmospheric tracer transport models: error characterization and propagation, Atmos. Chem. Phys., 8, 591–602, doi:10.5194/acp-8-591-2008, 2008.

Gerbig, C., Dolman, A. J., and Heimann, M.: On observational and modelling strategies targeted at regional carbon exchange over continents, Biogeosciences, 6, 1949–1959, doi:10.5194/bg-6-1949-2009, 2009.

Göckede, M., Michalak, A. M., Vickers, D., Turner, D. P., and Law, B. E.: Atmospheric inverse modeling to constrain regional-scale CO$_2$ budgets at high spatial and temporal resolution, J. Geophys. Res., 115, D15113, doi:10.1029/2009JD012257, 2010.

Gollehon, N. and Quinby, W.: Irrigation in the American West: Area, Water and Economic Activity, Int. J. Water Resour. Dev., 16, 187–195, doi:10.1080/07900620050003107, 2000.

Griffiths, A. D., Conen, F., Weingartner, E., Zimmermann, L., Chambers, S. D., Williams, A. G., and Steinbacher, M.: Surface-to-mountaintop transport characterised by radon observations at the Jungfraujoch, Atmos. Chem. Phys., 14, 12763–12779, doi:10.5194/acp-14-12763-2014, 2014.

Gurney, K. R., Mendoza, D. L., Zhou, Y., Fischer, M. L., Miller, C. C., Geethakuma, S., and de la Rue du Can, S.: High resolution fossil fuel combustion CO$_2$ emission fluxes for the United States, Environ. Sci. Technol., 43, 5535–5541, 2009.

Holton, J. R.: An introduction to dynamic meteorology, Academic Press, San Diego, 1992.

Huddleston, B., Ataman, E., de Salvo, P., Zanetti, M., Bloise, M., Bel, J., Franceschini, G., and d'Ostiani, L. F.: Towards a GIS-based analysis of mountain environments aand populations, Food and Agriculture Organization, Rome, 26, 2003.

Hurst, D., Lin, J. C., Romashkin, P., Gerbig, C., Daube, B. C., Matross, D. M., Wofsy, S. C., and Elkins, J. W.: Continuing emissions of restricted halocarbons in the USA and Canada: Are they still globally significant?, J. Geophys. Res., 111, D15302, doi:10.1029/2005JD006785, 2006.

IPCC: Climate Change 2014: Synthesis Report, Contribution of Working Groups I, II and III to the Fifth Assessment Report of the Intergovernmental Panel on Climate Change IPCC, Geneva, Switzerland, 151 pp., 2014.

Jeong, S., Zhao, C., Andrews, A. E., Bianco, L., Wilczak, J. M., and Fischer, M. L.: Seasonal variation of CH$_4$ emissions from central California, J. Geophys. Res.-Atmos., 117, D11306, doi:10.1029/2011JD016896, 2012.

Keeling, C. D., Bacastow, R. B., Bain-Bridge, A. E., Ekdahl, C. A., Guenther, P. R., Waterman, L. S., and Chin, J. F. S.: Atmospheric carbon dioxide variations at Mauna Loa Observatory, Hawaii, Tellus, 28, 538–551, 1976.

Kellndorfer, J., Walker, W., Kirsch, K., Fiske, G., Bishop, J., Lapoint, L., Hoppus, M., and Westfall, J.: NACP Aboveground Biomass and Carbon Baseline Data, V.2 (NBCD 2000), USA, 2000, ORNL Distributed Active Archive Center, 2013.

Kim, S. Y., Millet, D. B., Hu, L., Mohr, M. J., Griffis, T. J., Wen, D., Lin, J. C., Miller, S. M., and Longo, M.: Constraints on carbon monoxide emissions based on tall tower measurements in the U.S. Upper Midwest, Environ. Sci. Technol., 47, 8316–8324, 2013.

Knowles, J. F.: Spatio-temporal patterns of soil respiration and the age of respired carbon from high-elevation alpine tundra, PhD, Department of Geography, University of Colorado, Boulder, Boulder, Colorado, USA, 119 pp., 2015.

Lang, R. E., Sarzynski, A., and Muro, M.: Mountain megas: America's newest metropolitan places and a federal partnership to help them propser, Brookings Institute, Washington, DC, 64 pp., 2008.

Le Quéré, C., Moriarty, R., Andrew, R. M., Peters, G. P., Ciais, P., Friedlingstein, P., Jones, S. D., Sitch, S., Tans, P., Arneth, A., Boden, T. A., Bopp, L., Bozec, Y., Canadell, J. G., Chini, L. P., Chevallier, F., Cosca, C. E., Harris, I., Hoppema, M., Houghton, R. A., House, J. I., Jain, A. K., Johannessen, T., Kato, E., Keeling, R. F., Kitidis, V., Klein Goldewijk, K., Koven, C., Landa, C. S., Landschützer, P., Lenton, A., Lima, I. D., Marland, G., Mathis, J. T., Metzl, N., Nojiri, Y., Olsen, A., Ono, T., Peng, S., Peters, W., Pfeil, B., Poulter, B., Raupach, M. R., Regnier, P., Rödenbeck, C., Saito, S., Salisbury, J. E., Schuster, U., Schwinger, J., Séférian, R., Segschneider, J., Steinhoff, T., Stocker, B. D., Sutton, A. J., Takahashi, T., Tilbrook, B., van der Werf, G. R., Viovy, N., Wang, Y.-P., Wanninkhof, R., Wiltshire, A., and Zeng, N.: Global carbon budget 2014, Earth Syst. Sci. Data, 7, 47–85, doi:10.5194/essd-7-47-2015, 2015.

Levin, I. and Karstens, U. T. E.: Inferring high-resolution fossil fuel CO_2 records at continental sites from combined $^{14}CO_2$ and CO observations, Tellus B, 59, 245–250, doi:10.1111/j.1600-0889.2006.00244.x, 2007.

Lin, J. C.: Lagrangian modeling of the atmosphere: an introduction, in: Lagrangian Modeling of the Atmosphere, edited by: Lin, J. C., Brunner, D., Gerbig, C., Stohl, A., Luhar, A., and Webley, P., Geophysical Monograph, American Geophysical Union, 1–11, 2012.

Lin, J. C. and Gerbig, C.: Accounting for the effect of transport errors on tracer inversions, Geophys. Res. Lett., 32, L01802, doi:10.1029/2004GL021127, 2005.

Lin, J. C., Gerbig, C., Wofsy, S. C., Andrews, A. E., Daube, B. C., Davis, K. J., and Grainger, C. A.: A near-field tool for simulating the upstream influence of atmospheric observations: the Stochastic Time-Inverted Lagrangian Transport (STILT) model, J. Geophys. Res., 108, 4493, doi:10.1029/2002JD003161, 2003.

Lin, J. C., Gerbig, C., Wofsy, S. C., Andrews, A. E., Daube, B. C., Grainger, C. A., Stephens, B. B., Bakwin, P. S., and Hollinger, D. Y.: Measuring fluxes of trace gases at regional scales by Lagrangian observations: application to the CO_2 Budget and Rectification Airborne (COBRA) study, J. Geophys. Res., 109, D15304, doi:10.1029/2004JD004754, 2004.

Lin, J. C., Brunner, D., Gerbig, C., Stohl, A., Luhar, A. K., and Webley, P. W.: Lagrangian Modeling of the Atmosphere, in: Geophysical Monograph, American Geophysical Union, 349, 2012.

Mallia, D. V., Lin, J. C., Urbanski, S., Ehleringer, J., and Nehrkorn, T.: Impacts of upstream wildfire emissions on CO, CO_2, and $PM_{2.5}$ concentrations in Salt Lake City, Utah, J. Geophys. Res., 120, 147–166, doi:10.1002/2014JD022472, 2015.

Mell, W. E., Manzello, S. L., Maranghides, A., Butry, D., and Rehm, R. G.: The wildland-urban interface fire problem–current approaches and research needs, Int. J. Wildland Fire, 19, 238–251, 2010.

Mitchell, L. E., Lin, J. C., Bowling, D. R., Pataki, D. E., Strong, C., Schauer, A. J., Bares, R., Bush, S., Stephens, B. B., Mendoza, D., Mallia, D. V., Holland, L., Gurney, K. R., and Ehleringer, J. R.: Long-term urban carbon dioxide observations reveal spatial and temporal dynamics related to urban form and growth, P. Natl. Acad. Sci. USA, in review, 2017.

Monson, R. K., Turnipseed, A. A., Sparks, J. P., Harley, P. C., Scott-Denton, L. E., Sparks, K., and Huxman, T. E.: Carbon sequestration in a high-elevation, subalpine forest, Glob. Change Biol., 8, 459–478, 2002.

Monson, R. K., Lipson, D. L., Burns, S. P., Turnipseed, A. A., Delany, A. C., Williams, M. W., and Schmidt, S. K.: Winter forest soil respiration controlled by climate and microbial community composition, Nature, 711–714, 2006.

Mu, M., Randerson, J. T., van der Werf, G. R., Giglio, L., Kasibhatla, P., Morton, D., Collatz, G. J., DeFries, R. S., Hyer, E. J., Prins, E. M., Griffith, D. W. T., Wunch, D., Toon, G. C., Sherlock, V., and Wennberg, P. O.: Daily and 3-hourly variability in global fire emissions and consequences for atmospheric model predictions of carbon monoxide, J. Geophys. Res.-Atmos., 116, D24303, doi:10.1029/2011JD016245, 2011.

Negron, J. F., and Popp, J. B.: Probability of ponderosa pine infestation by mountain pine beetle in the Colorado Front Range, Forest Ecol. Manag., 191, 17–27, 2004.

Nehrkorn, T., Eluszkiewicz, J., Wofsy, S. C., Lin, J. C., Gerbig, C., Longo, M., and Freitas, S.: Coupled Weather Research and Forecasting–Stochastic Time-Inverted Lagrangian Transport (WRF–STILT) model, Meteorol. Atmos. Phys., 107, 51–64, 2010.

Parrish, D. D., Hahn, C. H., Fahey, D. W., Williams, E. J., Bollinger, M. J., Hübler, G., Buhr, M. P., Murphy, P. C., Trainer, M., Hsie, E. Y., Liu, S. C., and Fehsenfeld, F. C.: Systematic variations in the concentration of NO_x (NO Plus NO_2) at Niwot Ridge, Colorado, J. Geophys. Res.-Atmos., 95, 1817–1836, doi:10.1029/JD095iD02p01817, 1990.

Peters, W., Jacobson, A., Sweeney, C., Andrews, A. E., Conway, T. J., Masarie, K. A., Miller, J. B., Bruhwiler, L., Petron, G., Hirsch, A. I., Worthy, D., van der Werf, G. R., Randerson, J. T., Wennberg, P. O., Krol, M. C., and Tans, P. P.: An atmospheric perspective on North American carbon dioxide exchange: CarbonTracker, P. Natl. Acad. Sci., 104, 18925–18930, 2007.

Peters, W., Krol, M. C., Van Der Werf, G. R., Houweling, S., Jones, C. D., Hughes, J., Schaefer, K., Masarie, K. A., Jacobson, A. R., Miller, J. B., Cho, C. H., Ramonet, M., Schmidt, M., Ciattaglia, L., Apadula, F., Heltai, D., Meinhardt, F., Di Sarra, A. G., Piacentino, S., Sferlazzo, D., Aalto, T., Hatakka, J., StröM, J., Haszpra, L., Meijer, H. A. J., Van Der Laan, S., Neubert, R. E. M., Jordan, A., Rodó, X., Morguí, J. A., Vermeulen, A. T., Popa, E., Rozanski, K., Zimnoch, M., Manning, A. C., Leuenberger, M., Uglietti, C., Dolman, A. J., Ciais, P., Heimann, M., and Tans, P. P.: Seven years of recent European net terrestrial carbon dioxide exchange constrained by atmospheric observations, Glob. Change Biol., 16, 1317–1337, doi:10.1111/j.1365-2486.2009.02078.x, 2010.

Pillai, D., Gerbig, C., Ahmadov, R., Rödenbeck, C., Kretschmer, R., Koch, T., Thompson, R., Neininger, B., and Lavrié, J. V.: High-resolution simulations of atmospheric CO_2 over complex terrain – representing the Ochsenkopf mountain tall tower, Atmos. Chem. Phys., 11, 7445–7464, doi:10.5194/acp-11-7445-2011, 2011.

Potter, C., Fladeland, M., Klooster, S., Genovese, V., Hiatt, S., and Gross, P.: Satellite Data Analysis and Ecosystem Modeling for Carbon Sequestration Assessments in the Western United States, in: Carbon Sequestration and Its Role in the Global Carbon Cycle, American Geophysical Union, 89–99, 2013.

Ramankutty, N. and Foley, J. A.: Estimating historical changes in global land cover: Croplands from 1700 to 1992, Global Biogeochem. Cy., 13, 997–1027, doi:10.1029/1999GB900046, 1999.

Reisner, M.: Cadillac desert: The American West and its disappearing water, Penguin, 1993.

Rinsland, C. P., Mahieu, E., Zander, R., Demoulin, P., Forrer, J., and Buchmann, B.: Free tropospheric CO, C_2H_6, and HCN above central Europe: Recent measurements from the Jungfraujoch station including the detection of elevated columns during 1998, J. Geophys. Res.-Atmos., 105, 24235–24249, doi:10.1029/2000JD900371, 2000.

Rodenbeck, C.: Estimating CO_2 sources and sinks from atmospheric mixing ratio measurements using a global inversion of atmospheric transport, Max-Planck Institut fur Biogeochemie, Jena, Germany, 53 pp., 2005.

Rotach, M. W., Wohlfahrt, G., Hansel, A., Reif, M., Wagner, J., and Gohm, A.: The world is not flat: implications for the global carbon balance, B. Am. Meteorol. Soc., 95, 1021–1028, 2014.

Sarmiento, J. L., Gloor, M., Gruber, N., Beaulieu, C., Jacobson, A. R., Mikaloff Fletcher, S. E., Pacala, S., and Rodgers, K.: Trends and regional distributions of land and ocean carbon sinks, Biogeosciences, 7, 2351–2367, doi:10.5194/bg-7-2351-2010, 2010.

Schimel, D., Running, S., Monson, R., Turnipseed, A., and Anderson, D.: Carbon sequestration in the mountains of the Western US, Eos, 83, 445–456, 2002.

Schmidt, M., Graul, R., Sartorius, H., and Levin, I.: The Schauinsland CO_2 record: 30 years of continental observations and their implications for the variability of the European CO_2 budget, J. Geophys. Res.-Atmos., 108, 4619, doi:10.1029/2002jd003085, 2003.

Schwalm, C. R., Williams, C. A., Schaefer, K., Baldocchi, D., Black, T. A., Goldstein, A. H., Law, B. E., Oechel, W. C., Paw U, K. T., and Scott, R. L.: Reduction in carbon uptake during turn of the century drought in western North America, Nat. Geosci., 5, 551–556, doi:10.1038/NGEO1529, 2012.

Skamarock, W. C. and Klemp, J. B.: A time-split nonhydrostatic atmospheric model for weather research and forecasting applications, J. Comput. Phys., 227, 3465–3485, 2008.

Stephens, B. B., Gurney, K. R., Tans, P. P., Sweeney, C., Peters, W., Bruhwiler, L., Ciais, P., Ramonet, M., Bousquet, P., and Nakazawa, T.: Weak northern and strong tropical land carbon uptake from vertical profiles of atmospheric CO_2, Science, 316, 1732–1735, 2007.

Stephens, B. B., Miles, N. L., Richardson, S. J., Watt, A. S., and Davis, K. J.: Atmospheric CO_2 monitoring with single-cell NDIR-based analyzers, Atmos. Meas. Tech., 4, 2737–2748, doi:10.5194/amt-4-2737-2011, 2011.

Steyn, D., De Wekker, S. J., Kossmann, M., and Martilli, A.: Boundary Layers and Air Quality in Mountainous Terrain, in: Mountain Weather Research and Forecasting, edited by: Chow, F. K., De Wekker, S. F. J., and Snyder, B. J., Springer Atmospheric Sciences, Springer Netherlands, 261–289, 2013.

Sun, J. and De Wekker, S. F. J.: Atmospheric carbon dioxide transport over mountainous terrain, in: Mountain Ecosystems, edited by: Richards, K. E., Nova Science Publishers, 101–121, 2011.

Sun, J., Burns, S. P., Delany, A. C., Oncley, S. P., Turnipseed, A. A., Stephens, B. B., Lenschow, D. H., LeMone, M. A., Monson, R. K., and Anderson, D. E.: CO_2 transport over complex terrain, Agr. Forest Meteorol., 145, 1–21, doi:10.1016/j.agrformet.2007.02.007, 2007.

Sun, J., Oncley, S. P., Burns, S. P., Stephens, B. B., Lenschow, D. H., Campos, T., Monson, R. K., Schimel, D. S., Sacks, W. J., De Wekker, S. F. J., Lai, C. T., Lamb, B., Ojima, D., Ellsworth, P. Z., Sternberg, L. S. L., Zhong, S., Clements, C., Moore, D. J. P., Anderson, D. E., Watt, A. S., Hu, J., Tschudi, M., Aulenbach, S., Allwine, E., and Coons, T.: A multiscale and multidisciplinary investigation of ecosystem-atmosphere CO_2 exchange over the Rocky Mountains of Colorado, B. Am. Meteorol. Soc., 209–230, 2010.

Tkacz, B., Moody, B., Castillo, J. V., and Fenn, M. E.: Forest health conditions in North America, Environ. Pollut., 155, 409–425, doi:10.1016/j.envpol.2008.03.003, 2008.

Tuzson, B., Henne, S., Brunner, D., Steinbacher, M., Mohn, J., Buchmann, B., and Emmenegger, L.: Continuous isotopic composition measurements of tropospheric CO_2 at Jungfraujoch (3580 m a.s.l.), Switzerland: real-time observation of regional pollution events, Atmos. Chem. Phys., 11, 1685–1696, doi:10.5194/acp-11-1685-2011, 2011.

Urbanski, S. P., Hao, W. M., and Nordgren, B.: The wildland fire emission inventory: western United States emission estimates and an evaluation of uncertainty, Atmos. Chem. Phys., 11, 12973–13000, doi:10.5194/acp-11-12973-2011, 2011.

van der Molen, M. K. and Dolman, A. J.: Regional carbon fluxes and the effect of topography on the variability of atmospheric CO_2, J. Geophys. Res.-Atmos., 112, D01104, doi:10.1029/2006JD007649, 2007.

van der Werf, G. R., Randerson, J. T., Giglio, L., Collatz, G. J., Mu, M., Kasibhatla, P. S., Morton, D. C., DeFries, R. S., Jin, Y., and van Leeuwen, T. T.: Global fire emissions and the contribution of deforestation, savanna, forest, agricultural, and peat fires (1997–2009), Atmos. Chem. Phys., 10, 11707–11735, doi:10.5194/acp-10-11707-2010, 2010.

Wharton, S., Falk, M., Bible, K., Schroeder, M., and Paw U, K. T.: Old-growth CO_2 flux measurements reveal high sensitivity to climate anomalies across seasonal, annual and decadal time scales, Agr. Forest Meteorol., 161, 1–14, 2012.

Wiedinmyer, C. and Neff, J. C.: Estimates of CO_2 from fires in the United States: implications for carbon management, Carbon Balance Management, 2, 12 pp., doi:10.1186/1750-0680-2-10, 2007.

Yi, C., Anderson, D. E., Turnipseed, A. A., Burns, S. P., Sparks, J. P., Stannard, D. I., and Monson, R. K.: The contribution of advective fluxes to net ecosystem CO_2 exchange in a high-elevation, subalpine forest, Ecol. Appl., 18, 1379–1390, 2008.

Zardi, D. and Whiteman, C. D.: Diurnal Mountain Wind Systems, in: Mountain Weather Research and Forecasting, edited by: Chow, F. K., De Wekker, S. F. J., and Snyder, B. J., Springer Atmospheric Sciences, Springer Netherlands, 35–119, 2013.